Clays and Clay Minerals, Vol. 59, No. 3, 286–314, 2011.

MINERALOGICAL AND GEOCHEMICAL CHARACTERISTICS AND GENESIS OF THE SEPIOLITE DEPOSITS AT POLATLI BASIN (ANKARA, TURKEY)

MUAZZEZ ÇELIK KARAKAYA[1,*], NECATI KARAKAYA[1], AND ABIDIN TEMEL[2]

[1]Selçuk Üniversitesi Müh-Mim. Fak. Jeoloji Müh. Böl. Konya, 42075 Turkey
[2] Hacettepe Üniversitesi Müh. Fak. Jeoloji Müh. Böl. 06800 Beytepe Ankara, Turkey

Abstract—The Middle–Upper Miocene–Pliocene sediments near Polatlı contain commercial sepiolitic clay deposits. The sepiolite-rich Polatlı basin sediments were studied to describe the sepiolitic clay deposits of the area and to assess the environments of formation using X-ray diffraction, optical and scanning electron microscopy, and chemical analysis. The Polatlı basin is an elongated, rift-related graben trending NE–SW in central Turkey, filled with continental Late Miocene to Early Pliocene sediments. The sediments which comprise claystone, marl and limestone, dolostone, and evaporites are characteristic deposits of low-salinity, playa-lake depositional environments. These sepiolite-rich deposits include sepiolite, dolomite, and calcite, with minor amounts of palygorskite, quartz, moganite, amorphous silica (opal-CT), and feldspar.

The sepiolite shows all the characteristic X-ray diffraction reflections of that mineral, whereas amorphous silica containing sepiolite shows some of the characteristic reflections of sepiolite, but with somewhat broader and less intense basal reflections. In the siliceous deposits, the long, fibrous, and filamentous aggregates of the sepiolite were converted to thick, short fibers, low in Mg, and showing transition to amorphous silica.

Major and trace elements (*e.g.* Si, Al, Fe, Mg, Sr, Ba, *etc*.) were found almost exclusively in Mg-rich smectitic claystone and detrital silicate-rich rocks, whereas Mg, Ca, and some Si were concentrated in the neoformed minerals in the basin. The rare-earth elements (*REE)* and some of the high-field strength elements (HFSE), large ion lithophile elements (LILE), and transition elements (TRE) patterns were similar for detrital silicate-rich rocks and formed from neoformed mineral lithologies. The *REE*, TRE, LILE, and some of the HFSE contents of limestone, dolostone, and sepiolitic claystone were similar while those of detrital silicate-rich rocks and Mg-rich smectitic claystones were similar to each other. PAAS-normalized *REE* and other trace-element patterns were typically subparallel and depleted in neoformed minerals. All sample groups had positive Eu* anomalies, except Mg-rich smectite (0.80). Limestone, dolostone, and amorphous silica compounds showed slightly negative Ce* anomalies, whereas sepiolitic claystones, Mg-rich smectitic claystones, and detrital silicate-rich rocks had a slightly positive Ce* anomaly.

Key Words—Amorphous Silica, Dolomite, Mg-rich Smectite, Sepiolite, Polatlı, Turkey.

INTRODUCTION

The occurrence of sepiolite in sediments is generally considered to be diagnostic of highly saline and alkaline environments. Because fibrous clay minerals are of great economic interest and have many industrial applications, sepiolite occurrences have been studied in the USA, Kenya, Spain, Portugal, Turkey, Saudi Arabia, Great Britain, and Morocco among others (Post, 1978; Galán and Ferrero, 1982; Gençoğlu and İrkeç, 1994; Torres-Ruíz *et al*., 1994; Mayayo *et al*., 1998; Ece and Çoban, 1994; Çoban, 2001; Kadir *et al*., 2002; Karakaya *et al*., 2004; Yalçın and Bozkaya, 1995; Yalçın and Bozkaya, 2004). Turkish sepiolites have been found in the Eskişehir, Konya, Bolu, and Ankara regions of northwest Anatolia.

* E-mail address of corresponding author:
mzzclk@hotmail.com
DOI: 10.1346/CCMN.2011.0590306

In the study area, Late Miocene–Early Pliocene sediments consist of mudstones, marls, limestones, dolostones, and gypsiferous deposits interfingerred with clastic marginal lake facies and alluvial deposits. The economically valuable sepiolite deposits in the investigation area had not previously been discovered. The nearly pure sepiolitic layer varies from 0.1 to 5 m thick and from 50 to 100 m in lateral extent. An operating license has been granted and mining will commence in the near future. The Eskişehir sepiolite deposits are well known, and the second largest bedded and nodular type sepiolite occurrences are located in southeast Eskişehir (Ece *et al*., 2003). Features of the Eskişehir deposit have been published by many investigators, *e.g.* Ece and Çoban (1994), Çoban (2001), and Kadir *et al*. (2002).

Miocene sepiolite deposits of fluvio-lacustrine origin formed in a closed alkaline, shallow-lake environment in the vicinity of Eskişehir (Figure 1). Miocene lacustrine sepiolites were formed as stratiform and nodular masses (Ece and Çoban, 1994). The sepiolite interbedded with

https://doi.org/10.1346/CCMN.2011.0590306 Published online by Cambridge University Press

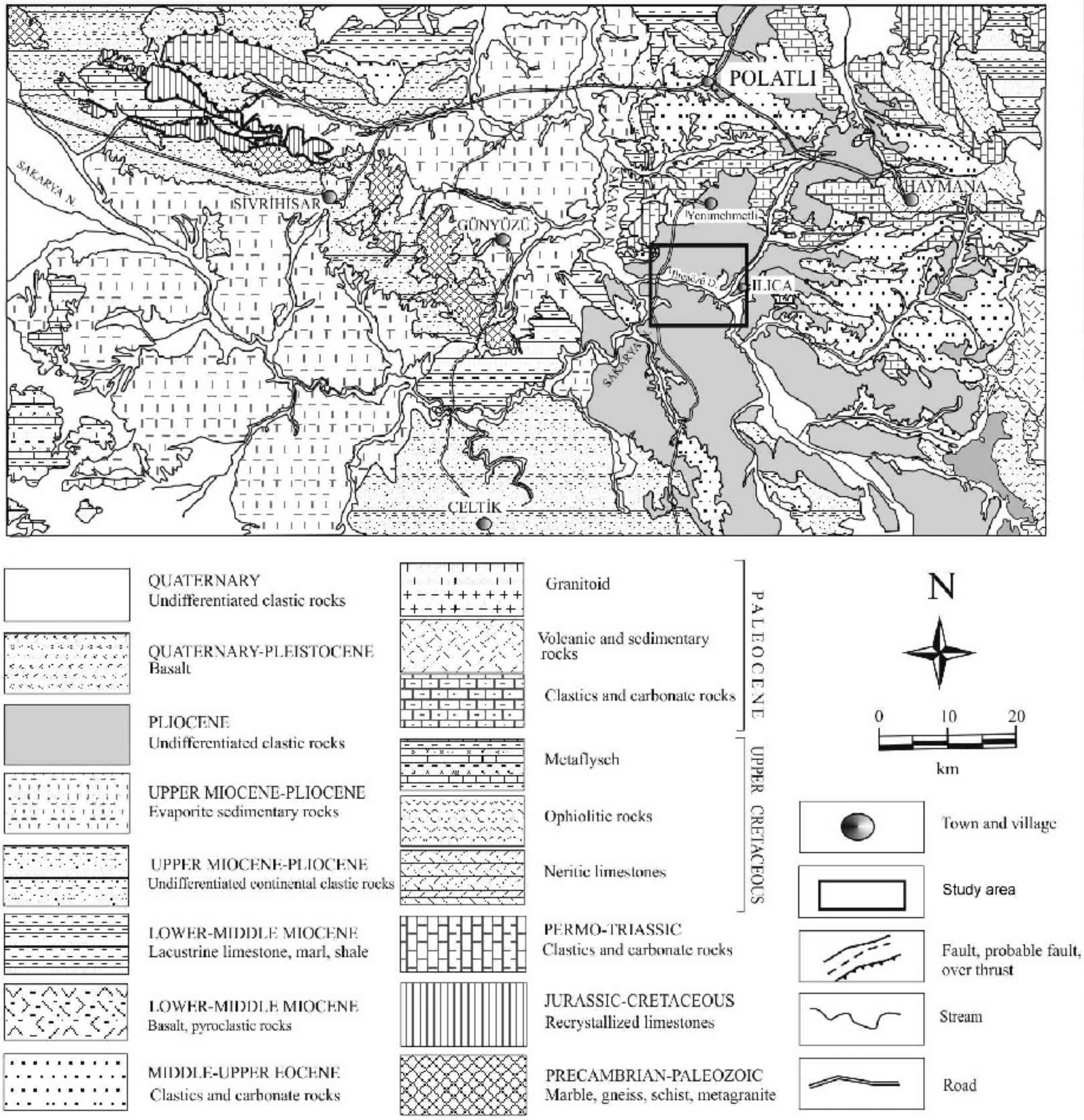

Figure 1. Detailed geologic map of the Sakarya basin, central Anatolia, Turkey (simplified from a 1:500,000 scale map – MTA, 2001).

dolomite, dolomitic marl, calcareous clay, clayey limestone, and gypsum, precipitated directly from lake water, and the sepiolite nodules formed as a diagenetic replacement of magnesite pebbles. In the Konya-Karapınar basin, sepiolite occurrences display similarities to Eskişehir sepiolites (Karakaya *et al*., 2004). Those authors argued that Karapınar sepiolites were formed either by conversion of dolomite or by direct precipitation from solution under alkaline and saline conditions.

Sepiolite enrichments in nature are of two types, both of which are found in Eskişehir region. The first is known as meerschaum while the other is referred to as 'industrial or layered' sepiolite, also known as sedimentary sepiolite. The meerschaum has been mined since 1890 and the sedimentary sepiolite since 1985. The sedimentary sepiolite is similar in some regards to those investigated in the present study. Eskişehir sepiolites were formed in Middle to Upper Miocene lacustrine sediments while Polatlı sepiolites formed during the Early Pliocene. Nodular sepiolites and magnesite occurrences were not observed in the study area. The trace-element chemistry of the sepiolite occurrences and relationships among the silica layers/nodules, Mg-rich smectite beds, and sepiolite-dolomite formations were not previously investigated in detail.

https://doi.org/10.1346/CCMN.2011.0590306 Published online by Cambridge University Press

The present study aimed to: (1) investigate the mineralogical and geochemical relations of the calcareous lacustrine sediments to sepiolite deposits; (2) explain the origins of sepiolite and Mg-rich smectite, and amorphous silica occurrences; and (3) compare some features of the Polatlı sepiolites with those of the Eskişehir sepiolites.

GEOLOGIC SETTING

The study area is located in the southeastern part of the Sakarya basin, which is partially surrounded by Upper Paleozoic metadolomitic limestone, Upper Cretaceous ultramafic rocks, and Paleocene volcanic rocks, granitoids, and carbonates (Figure 1). The Upper Paleozoic metamorphic rocks are the oldest unit of the basin, and consist of mica schists, phyllites, metasandstones, and metadolomitic limestones. Upper Cretaceous ultramafic rocks were covered by an alkaline and sulfate-bearing lake ~200 km long and 100 km wide during Early Miocene to Pliocene times (Ece and Çoban, 1994). The basin developed a rift-related graben structure by the time of the Oligocene–Miocene transition. The Upper Cretaceous ultrabasic rocks are composed of an ophiolitic *mélange* including gabbro, pyroxenite, dunite, and peridotite rocks that have been overturned upon the Paleozoic metamorphic rocks (Asutay *et al*., 1989) (Figure 1). The Late Cretaceous–Paleocene plutonic rocks consist of granite and micaceous and porphyritic granodiorites. These rocks are in turn overlain unconformably by Late Miocene–Early Pliocene volcanic, volcanoclastic, and fluvio-lacustrine sedimentary rocks. The volcanic rocks are made up mainly of tuffs and a minor amount of volcanic breccia, agglomerate, and lava flow material. The volcanic rocks are basaltic, trachytic, and trachyandesitic in composition and erupted in different episodes. The age of the volcanic rocks was defined by Temel *et al*. (2010), using K-Ar dating, as Early–Middle Miocene. The volcanics, located in the Balkuyumcu and Polatlı regions (SW of Ankara), consist of basaltic andesitic, andesitic, dacitic, and rhyolitic rocks extruded during the Early Miocene (14–22 Ma) (Varol *et al*., 2007; Temel *et al*., 2010).

The volcano-sedimentary units show cyclic sedimentation, and consist mainly of silts, clays, limestones, dolostone, and tuffaceous, evaporitic, and silicified sediments. The clay section, which consists of green and yellow illitic and smectitic layers, contains different sized gypsum (1–10 cm) crystals and limestone interbeds (5–6 m), deposited in alternating layers, generally at the base of the succession. Above the base, limestone and marl beds are composed of calcite, dolomite, sepiolite, and sepiolite-bearing dolomite/calcite (Figure 2). Abundant (30–50% of sediments) and large (0.1 mm–2 cm) gastropod and ostracod fossils were observed in the upper horizons of the stratigraphic sequence deposited in the fluvio-lacustrine basin. The presence of the fossils indicates closing of the basin implying a relatively closed basin without water recharge at the end of Early Pliocene.

Three different types of sepiolite beds have been recognized in the study area: (1) organic matter-rich black sepiolite beds (total organic carbon, TOC, ≈2.56–5.69%) formed in a deep part of the basin; (2) organic matter-poor brown sepiolite beds, containing ~5% dolomite, often overlying the first bed; and (3) white, cream, or beige dolomite/calcite-(~20–40%) bearing sepiolite beds (Figure 3a). These types of sepiolite beds were also defined northwest of the Sakarya basin by Bellanca *et al*. (1993), Ece and Çoban (1994), and Kadir *et al*. (2002).

Silica enrichments were observed in two types of occurrence: (1) glassy, brown, pale brown, or blackish brown chert beds (5 cm–2 m thick) and lenses (2–20 cm thick); and (2) chert nodules 1–3 cm in radius with white carbonate-rich (mainly Mg) exterior rims and a beige translucent interior (Figure 3b,c). The chert layers/lenses are distributed irregularly and discontinuously within and mainly overlying the sepiolitic clay beds and was observed over an area of ~100–2000 m^2. Sometimes, thin, black, brown-beige chert beds (1–50 cm thick) were interlayered with the sepiolite or sepiolite-bearing dolomitic limestone beds, indicating that siliceous gel precipitated from supersaturated solution during and after sepiolite precipitation, and then converted diagenetically to opal-CT and other silica minerals. The dolostone-covered chert nodules were generally formed above the nearly pure dolostone (Figure 3b–d).

MATERIALS AND METHODS

Sixty-eight representative samples were collected from 11 sections in the study area (Figure 2). All samples were ground gently for 5 min in a porcelain ball mill for X-ray diffraction (XRD) and chemical analysis. Mineralogical analyses of the samples were performed on randomly oriented samples (total fraction) and on the clay (<2 μm) fraction using XRD (Rigaku D/MAX 2200 PC, CuKα radiation with tube voltage and current of 40 kV and 40 mA, respectively) with a scanning speed of 2º/min from 2 to 70º2θ, at Hacettepe University (Ankara). The powder samples were placed in a beaker, covered with distilled water, and immersed in an ultrasonic bath. Carbonate-rich and marl samples were decomposed in dilute HCl acid (5% HCl) at 30ºC (Jackson, 1975). The acid was added slowly to the sample beaker until the reaction stopped. Then the sample was washed several times with distilled water and transferred to a measuring cylinder; 500 mL of deionized water was added to the sample. The <2 μm clay fraction was obtained by gravitational sedimentation of the purified samples. The <2 μm clay fraction was then separated by centrifugation from the water.

https://doi.org/10.1346/CCMN.2011.0590306 Published online by Cambridge University Press

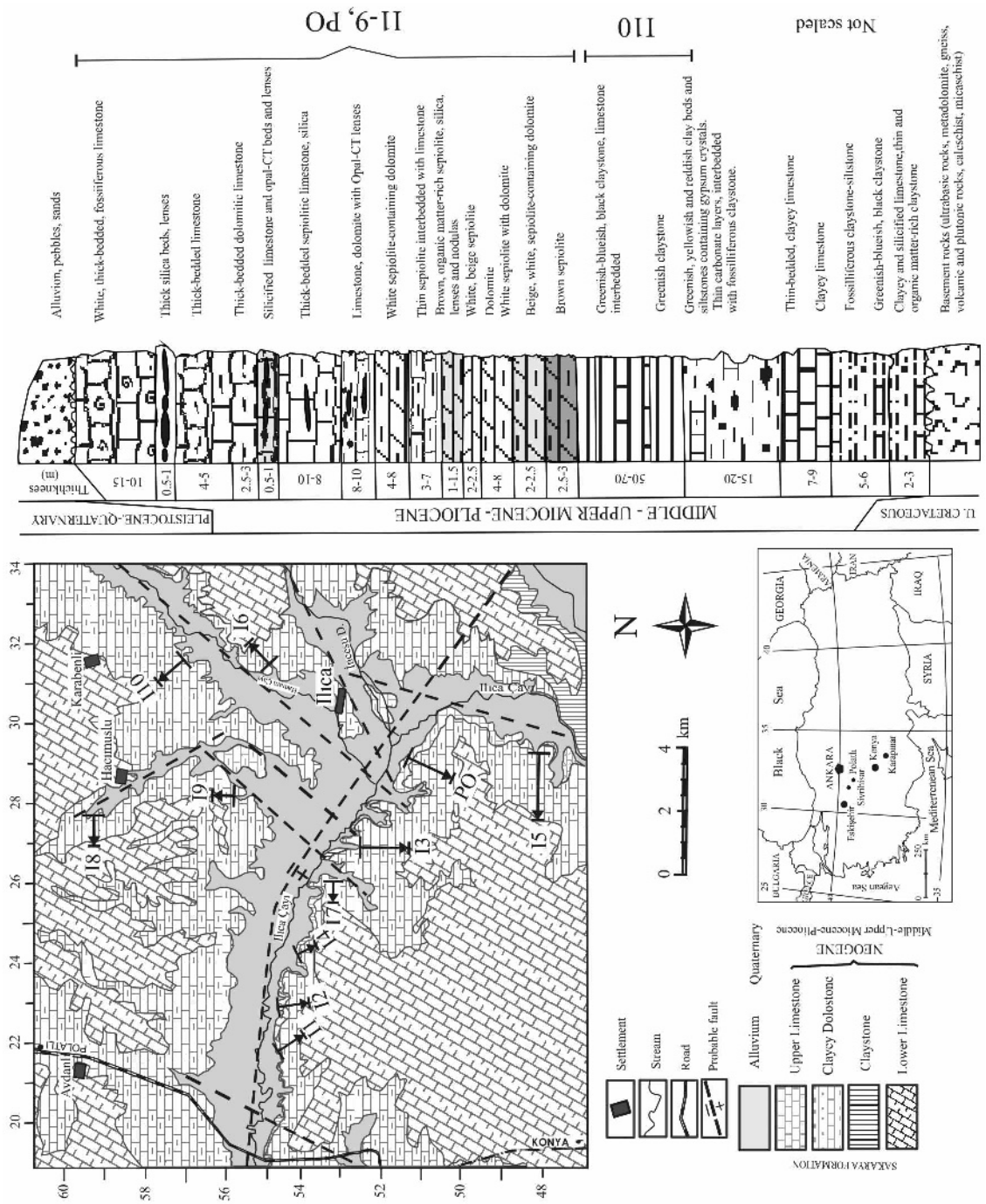

Figure 2. Detailed geologic map, locations of measured sample sections, and generalized stratigraphic section of the investigation area.

https://doi.org/10.1346/CCMN.2011.0590306 Published online by Cambridge University Press

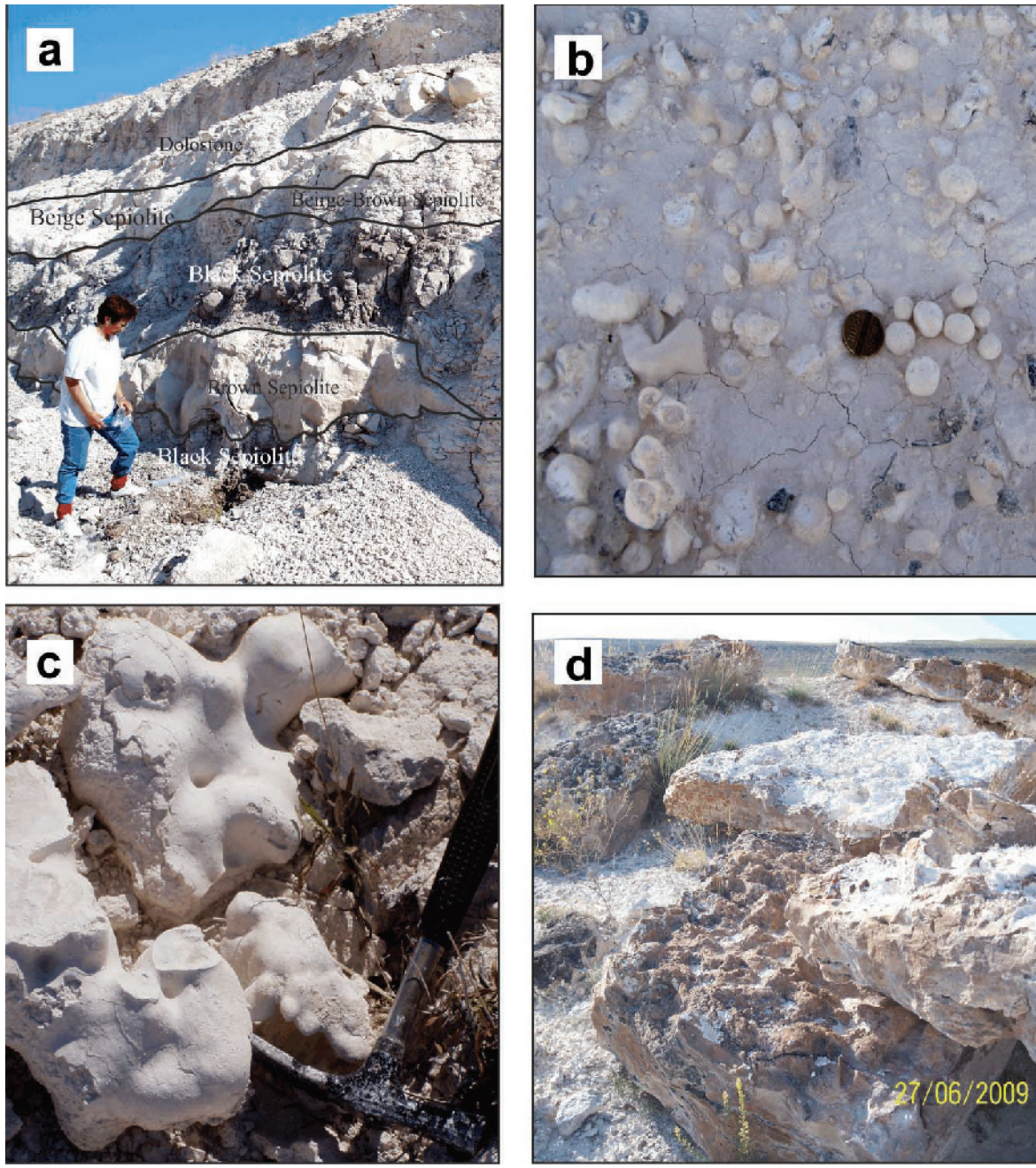

Figure 3. Field photographs of sepiolite and different types of siliceous deposits in the study area. (a) From bottom to top, black sepiolite, brown sepiolite, and beige-white sepiolite covered by dolostone. (b) Spherical, silica-rich nodules. The interior of the nodules consists mainly of SiO_2, while the exterior (3−5 mm thick) is of MgO. (c) Different form of silica-rich material: the composition of this material is the same as that of the nodules. (d) Glassy, brown, and pale-brown silica beds which contain mainly moganite and quartz while other beds contain opal-A and opal-CT. The siliceous beds and nodules were generally found to occur above the sepiolite and sometimes sepiolite-dolostone layers.

After removing non-silicate minerals, *e.g.* calcite and dolomite, from the clay-sized fractions, three specimens for XRD analysis were prepared for each sample by sedimentation onto glass slides with air drying at 25ºC, then subjected to (1) no further treatment, (2) ethylene-glycol solvation, or (3) heating at 490ºC for 4 h. The mineral proportions were determined from the powder XRD patterns following a standard method developed by Temel and Gündoğdu (1996) and combined chemical analysis (Table 1). In this method, all samples were mounted in the same way and the characteristic peak intensities (I) of minerals were normalized to that of the

https://doi.org/10.1346/CCMN.2011.0590306 Published online by Cambridge University Press

Table 1. Mineral assemblages and abundance of minerals (wt.%) in the basin as inferred from mineralogical and chemical analysis results (rare components omitted).

Samples	Dol	Cal	Sep	Qz/Mog	Sme	Mg-Sme	Ilt	Kln	Fsp	Plg	Opl-Trd	Ilt-Sme	Gp
I1-8/1	98			2									
I1-8/2	98			2									
I1-19	5	3		15	42		25	2	8				
I1-23	4	18		15	27		20	3	8			5	
I1-25	4	19		7	32		22	2	8			6	
I2-4	99			1									
I3-3	1	97		1						1			
I3-5	1	97		1						1			
I3-8	1	98		1									
I3-11	2	97		1									
I3-14	4	25		11	16		27	2	10			5	
I3-15	4	28		10	15		28	2	10			3	
I3-18	5	26		10	15		28	2	11			3	
I3-21	4	11		16	33		20	3	8			5	
I3-22	4	11		20	29		20	3	8			5	
I3-25	2	96		2									
I3-28	12	86		2									
I3-30	4	12		17	29		20	3	10			5	
I3-31	2	96		2									
I3-32	94	4		2									
I3-33		95		5									
I3-34		99		1									
I3-38	5	95		1									
I4-0	99			1									
I4-1	99			1									
I4-5	2	2	94							2			
I4-6	3	2	96										
I4-8	98		1	1									
I4-14	98			2									
I4-27	4			14	42		23	3	9				5
I4-31	1	97		2									
I4-33	2	97		1									
I4-34	3	96		1									
I5-5	4	12		18	29		20	3	9			5	
I5-16	97		2	1									
I5-20	97		2	1									
I5-21	4	15		16	26		22	3	9			5	
I6-1		96		4									
I7-2	2	1	97										
I7-4			100										
I7-5			100										
I7-9			100										
I7-11	98			2									
I7-13			100										
I7-19			100										
I9-1			100										
I9-4			100										
I9-6	98			2									
I9-13	4	3		14	41		24	2	7			5	
I9-16		98		2									
I10-1		1	96							3			
I10-3			98							2			
I10-4			100										
I10-8	13										87		
I10-9	2		24								74		
I10-12	2										98		
I11-17						100							
I11-27						100							
I11-37						100							
PO-1	10		85							5			
PO-3			95							5			
PO-4			100										
PO-8													
PO-9			35	65									
PO-12				100									

Dol: Dolomite, Cal: calcite, Sep: sepiolite, Qz: Quartz, Sme: smectite, Mog: Moganite; Mg-Sme: Mg-rich smectite, Ilt: Illite, Kln: kaolinite, Fsp: Feldspar, Plg: Palygorskite, Opl-Trd: Opal-CT, Ilt-Sme: Illite-Smectite, Gp: Gypsum (abbreviations from Whitney and Evans, 2010).

https://doi.org/10.1346/CCMN.2011.0590306 Published online by Cambridge University Press

(104) reflection of dolomite. In other words, a K factor for each mineral (including clays with peaks between 19 and 20º2θ) was determined as $K = I_{dolomite}/I_{mineral}$ in a 1:1 dolomite-mineral mixture by weight. Percentages of the minerals were calculated from the following equation: % of mineral a = $(100 \times K_a \times I_a)/(K_a \times I_a + K_b \times I_b + ...K_n \times I_n)$. The accuracy of the mineral abundance determinations was ±5%.

The size and morphological features of submicroscopic clay minerals and their interrelations with other minerals were determined using scanning electron microscopy (SEM) and energy dispersive X-ray spectroscopy (EDS) for elemental composition, using facilities at the Afyonkarahisar Kocatepe University (LEO 1430VP SEM with EDS and BSE; accelerating voltage was in the range 15–20 kV, with a probe current of 15 μA and a spot size of 5 μm to identify mineral composition). The sample was dispersed over a sample holder and gold-sputtered for EDS analysis. The samples were dried at 50ºC for 1 h and coated with gold to a thickness of 5 μm. A ZAF calculation programme was used to calculate the wt.% of major oxides at each point. The total abundances of the major oxides and minor, rare-earth, and refractory elements were performed by ACME Laboratories (Vancouver, British Columbia, Canada), using inductively coupled plasma optical emission spectrometry and mass spectrometry (Spectro ICP-OES and Perkin Elmer ELAN 9000 ICP-MS, USA, respectively). Samples (0.1 g) were fused in Li-metaborate/tetraborate and digested with nitric acid. Loss on ignition (LOI) was determined by weight difference after ignition at 1000ºC. Total organic carbon (TOC) and sulfur were also measured by ACME Laboratories (Leco CS230). In addition, a separate 0.5 g portion of each sample was digested in Aqua Regia and analyzed by ICP-MS for precious and base metals, *e.g.* Al, Fe, Ti, Co, Cd, Zr, Ga, Nb.

RESULTS

Mineralogy

The mineral assemblages of the samples, determined by XRD, were relatively homogenous, although the mineral proportions are extremely variable (Table 1, Figure 4). The mineral associations of the samples were classified in two different groups: (1) detrital silicate-rich rocks: smectite, illite, kaolinite, interstratified illite-smectite, quartz, and feldspar; (2) neoformed minerals: mainly sepiolite, dolomite and/or calcite, silica compounds (amorphous and/or crystalline), Mg-rich smectite, and scarce palygorskite and aragonite. Detrital silicate-rich rocks deposited in shallow areas of the basin originated from source rocks which cropped out in the area surrounding the basin. Samples from the area were grouped as dolostone, limestone, sepiolitic claystone, Mg-rich smectitic claystone, silica-rich rocks, and detrital silicate-rich rocks.

The samples from the middle part of the succession, in particular, are rich in sepiolite, with its contents reaching 100% in some cases, and palygorskite comprises no more than ~10% (Figures 2, 3a; Table 1). The black sepiolite layers contain a minor amount of palygorskite, whereas the brown to beige sepiolite horizons do not. The black sepiolite horizons are richer in organic matter than the other sepiolitic layers. The white sepiolite deposits are generally found together with dolostone above the brown-beige sepiolite beds, whereas limestones contain sepiolite at the mid-levels of the basin (Figure 3a). The sepiolite content of the limestones is less than that of the dolostones. Although dolostones are sometimes nearly pure dolomite, in some samples the dolomite was most commonly observed with sepiolite and sometimes with calcite or calcite+sepiolite+quartz. Calcite is generally found at the upper levels of the section. The most abundant detrital minerals in the detrital silicate-rich rocks are quartz, feldspar, mica, and rarely smectite, illite, and kaolinite which reach proportions of up to 70%.

The amorphous silica beds and lenses, as well as nodules of various shapes, are composed of quartz, moganite, and some opal-CT. Outer parts of the silica nodules and opal lenses have thin (1–2 mm, Figure 3b,c) coatings of carbonate minerals, mainly dolomite. Amorphous silica was determined at significant quantities sometimes within and sometimes over sepiolite layers. The XRD reflections of moganite at 2.88, 3.11, 3.33, 3.39, and 4.45 Å were strong in the silica-rich samples (Figure 4). Opal-CT is characterized by a strong XRD reflection at 4.07 Å (with a shoulder near 4.30 Å) and a weaker reflection at 2.50 Å (Figure 4). Identification of opal-A from XRD data is difficult, particularly in the presence of large quantities of opal-CT. The broadening of the reflection at ~4.10 Å suggested the presence of at least a small amount of opal-A.

Mineralogical study of the Polatlı sepiolites revealed just one reflection at 12.07 Å corresponding to the (110) reflection of phyllosilicates; even though the reflection was very intense, no differences among the sepiolitic samples were observed in terms of the sharpness of the reflections or other characteristics (Figure 4). After saturation with ethylene glycol, the reflection at 12.40 Å remained, but expanded slightly (Figure 5a). Heat treatment at 490ºC caused this line to shift to 10.40 Å. These data identified the mineral as sepiolite. The sharpness (width at half height) of the reflections in XRD revealed an ordered structural arrangement of the sepiolite. Similar properties were also observed in the Eskişehir (Ece and Çoban, 1994) and Konya sepiolites (Karakaya *et al*., 2004). Sharper peaks in the powder XRD traces of unoriented samples (Figure 4) suggested that the crystallinity of the sepiolite from the Polatlı area was better developed than the crystallinity of sepiolites of the Eskişehir (Ece & Çoban, 1994) and Yunak (Yeniyol,

https://doi.org/10.1346/CCMN.2011.0590306 Published online by Cambridge University Press

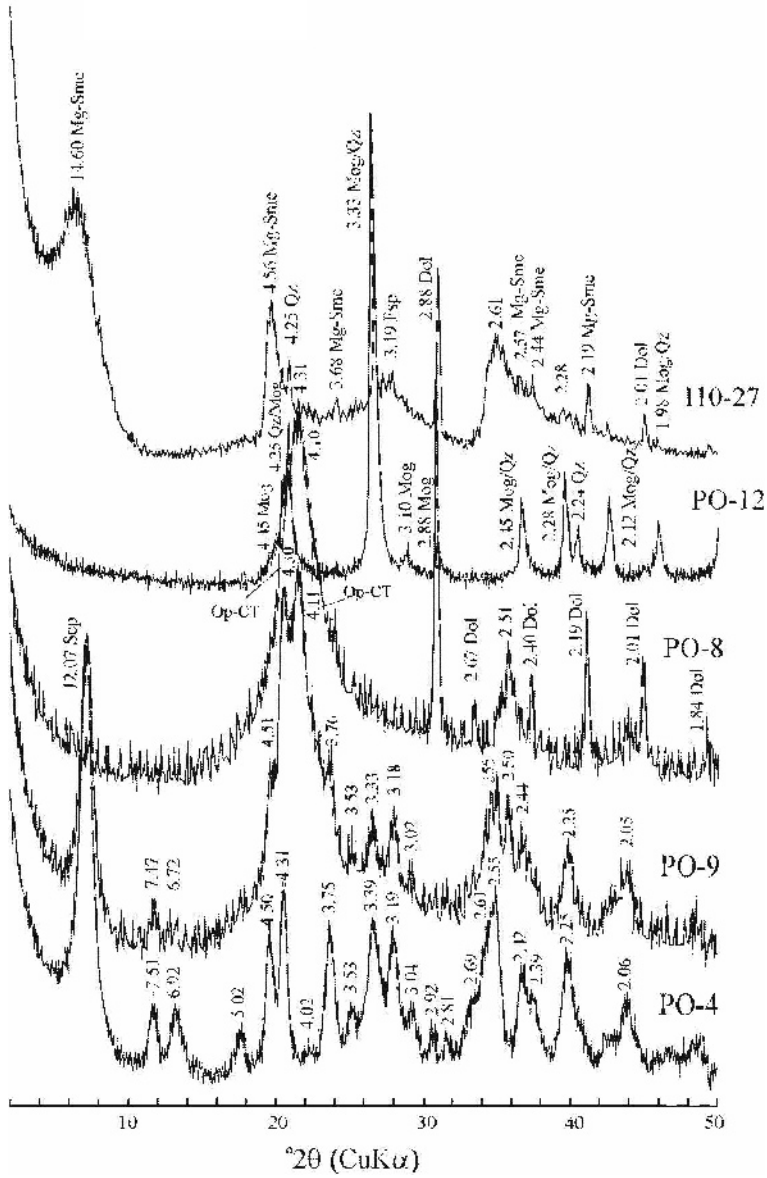

Figure 4. XRD patterns of random powder bulk samples showing the main reflections (Å) and minerals identified in some of the samples. Dol: dolomite, Qz: quartz, Sp: sepiolite, Mg-Sme: Magnesium-rich smectite, Op-CT: opal-CT, Mog: moganite, Fsp: Feldspar. PO-4 and PO-9 are beige and white sepiolite, respectively (abbreviations from Whitney and Evans, 2010).

1986) deposits. Quantitative estimation of sepiolite in the sepiolitic claystone indicated that it made up 100% of the clay fraction and, as a result, it made up between 10% and 100% of the whole-rock sample. The white sepiolitic claystone contains less sepiolite than the other types of sepiolitic claystone. Characteristic reflections of sepiolite were poorly defined in amorphous silica-rich samples, and the reflections were seen as continuous diffraction bands. In addition, the basal reflection is became somewhat broader and less intense. Palygorskite was mainly observed at the bottom layers of the section within the black sepiolite layers. The basal reflection (110) of palygorskite was observed at 10.80 Å. The location of the (110) reflection of palygorskite was shifted to 10.13 Å after heat treatment. Following glycolation, no swelling was noted in the palygorskite. Mg-rich smectite appeared to consist of a single, uniform clay species and gave clearly separated basal spacings. The first-order basal spacing at 14.73 Å for the Mg-rich smectite shifted to form a very strong, sharp reflection at 17.67 Å when the Mg-rich smectite was solvated with ethylene glycol. When the Mg-rich smectite was heated at ~490°C, the 14.73 Å reflection shifted to 10.06 Å because of loss of interlayer water while retaining the

https://doi.org/10.1346/CCMN.2011.0590306 Published online by Cambridge University Press

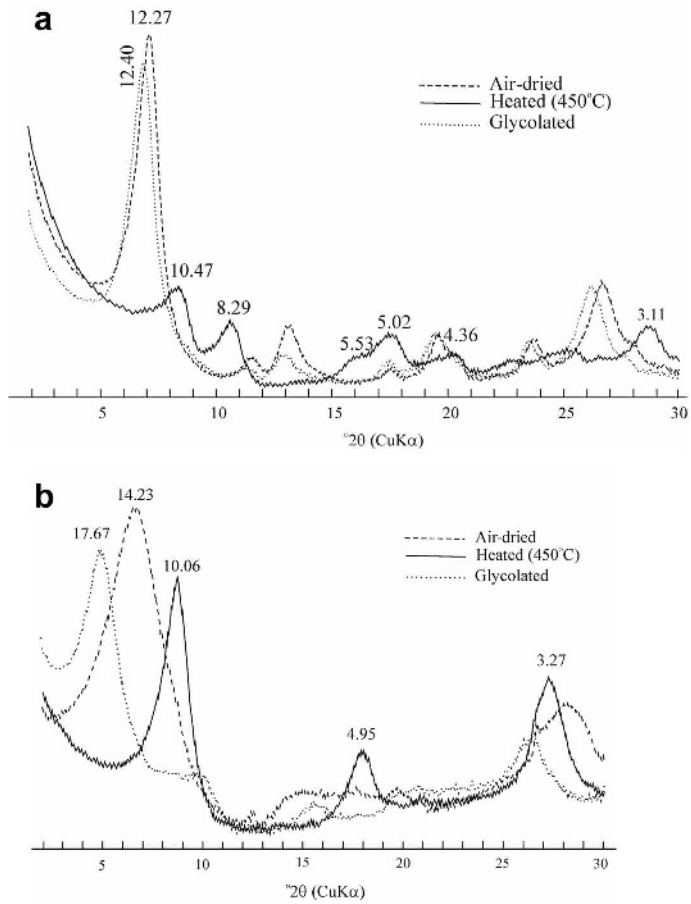

Figure 5. XRD pattern of <2 μm fraction (oriented under ambient conditions, after heating to 490ºC and solvation in an ethylene glycol atmosphere): (a) black sepiolite (PO-3), (b) Mg-rich smectite.

intensity of the reflection (Figure 5b). The d_{060} reflection at 1.53 Å of the smectite pointed to an octahedral composition rich in Mg.

Observations by SEM

Morphological features and the fabric of clay minerals, dolomite, calcite, and silica minerals were examined *via* SEM-EDS. The SEM studies were performed on whole-rock samples, and the studies revealed that the texture of the fibrous phyllosilicates is extremely variable. The most common texture for all types of sepiolite was a chaotic ordering of the sepiolite fibers. The study by SEM-EDS of sepiolite revealed several mineralogic and chemical details. First, the more abundant morphologies corresponded to woollen-ball-like aggregates forming grains up to 10−20 μm long, and <1 μm thick (Figure 6a). Next, the sepiolite occurred sporadically as planar aggregates (often with filamentous borders) and filamentous-fibrous aggregates with bundle-like aspects (Figure 6b,c). The palygorskite crystals formed fibrous aggregates similar to those of sepiolite but of larger fiber size, sometimes reaching 60 μm in length. Palygorskite fibers contained much more Al than sepiolite in EDS analyses (Figure 6d,e, Table 3). Finally, some of the sepiolite fiber bunches grew on the edges or voids of euhedral to subhedral dolomitic rhombs, probably derived from the sepiolite fibers or they precipitated together. Alternatively, sepiolite developed as a coating on or surrounding dolomite rhombs. Sepiolite fibers were also observed on the surfaces of dolomites with rhombohedral morphology. The sizes of dolomite rhombs were 0.5−1.0 μm (Figure 6f,g). Partly dissolved euhedral−subhedral calcite crystals were replaced by sepiolite fibers. Also, some calcite crystals showed transformation to skeletal calcite (Figure 6h,i, Table 3). Mg-rich smectite occurred as thin, leaf-shaped crystals in a dense aggregate honeycomb texture with platy and oriented smectite particles (Figure 6k, Table 3).

The opal and quartz (chalcedony) were observed in cavities of the sepiolitic claystone. Analysis by SEM revealed that opal consisted of spherical particles of amorphous silica ~0.5 μm in diameter (opal-A; Florke *et al*., 1991) and opal-CT lepispheres (Wise and Kelts, 1972) 0.5−2.0 μm in diameter, which were aggregates of small, hexagonal, and blade-shaped quartz crystals (Figure 7a−c, Table 3). Several relatively large, platy

https://doi.org/10.1346/CCMN.2011.0590306 Published online by Cambridge University Press

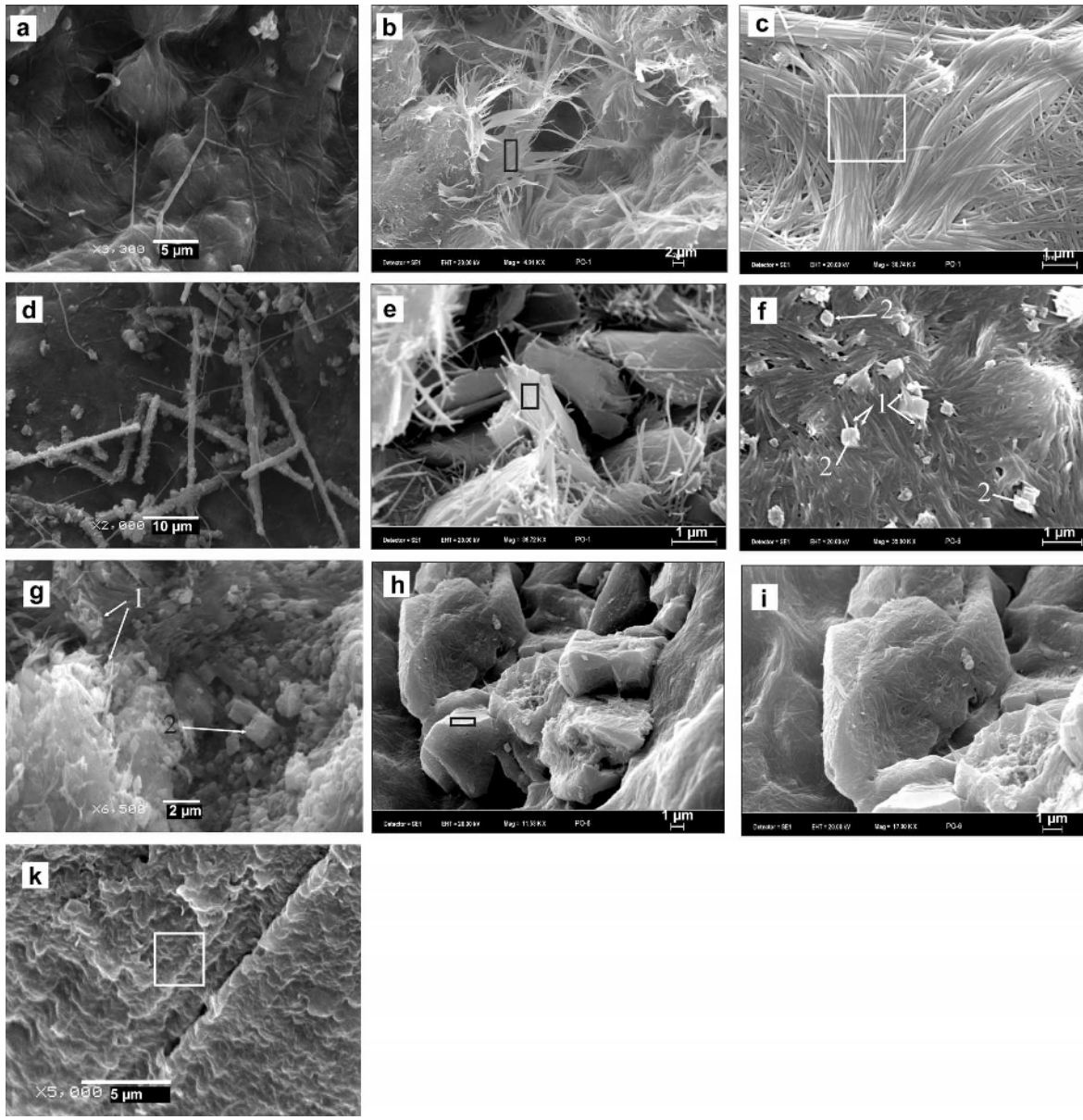

Figure 6. (a) SEM image showing woollen-ball-like aggregates forming grains up to 10–20 µm long and <1 µm thick. (b,c) The sepiolite, which lies in parallel planes, consists of closely bunched fibers (often with filamentous borders). (d,e) The palygorskite crystals form fibrous aggregates similar to those of sepiolite but with a larger fiber size, sometimes reaching up to 60 µm in length and containing much more Al than the sepiolites. (f,g) The bunches of sepiolite fibers grew on the edges or voids of euhedral to subhedral dolomitic rhombs, or they developed as a coating (indicated by arrow 1). Most of the palygorskite fibers in part d were covered by calcite and/or dolomite rhombs. The dolomite rhombs are 0.5–2 µm across (f,g) and show secondary coating or growth texture (indicated by arrow 2). (h,i) Euhedral-subhedral and partly dissolved calcite crystals have been replaced by sepiolite fibers. The calcite crystals were also transformed to skeletal calcite and some parts/faces of the calcites were replaced by sepiolite fibers. The outer sides of the calcite crystals contain mostly CaO (89.9%, Table 3) and their inner sides consist of fibrous sepiolite. The relation between dolomite and sepiolite indicates that these minerals may have developed together. (k) Mg-rich smectite occurs as thin, leaf-shaped crystals in a dense aggregate that displays a honeycomb texture with platy and oriented smectite particles. The area analyzed using EDS is indicated by a square.

silica particles, up to 0.5–1.0 µm across, exhibited a continuous transition between amorphous silica (opal-A) and crystallized quartz. The particles consisted of several closely stacked, thin lamellae, with pseudo-hexagonal shapes 200–300 nm wide (Figure 7d). These amorphous domains contained rounded zones suggesting intergrowth of rounded disks 20–50 µm in diameter. The lamellae containing crystalline silica generally displayed

https://doi.org/10.1346/CCMN.2011.0590306 Published online by Cambridge University Press

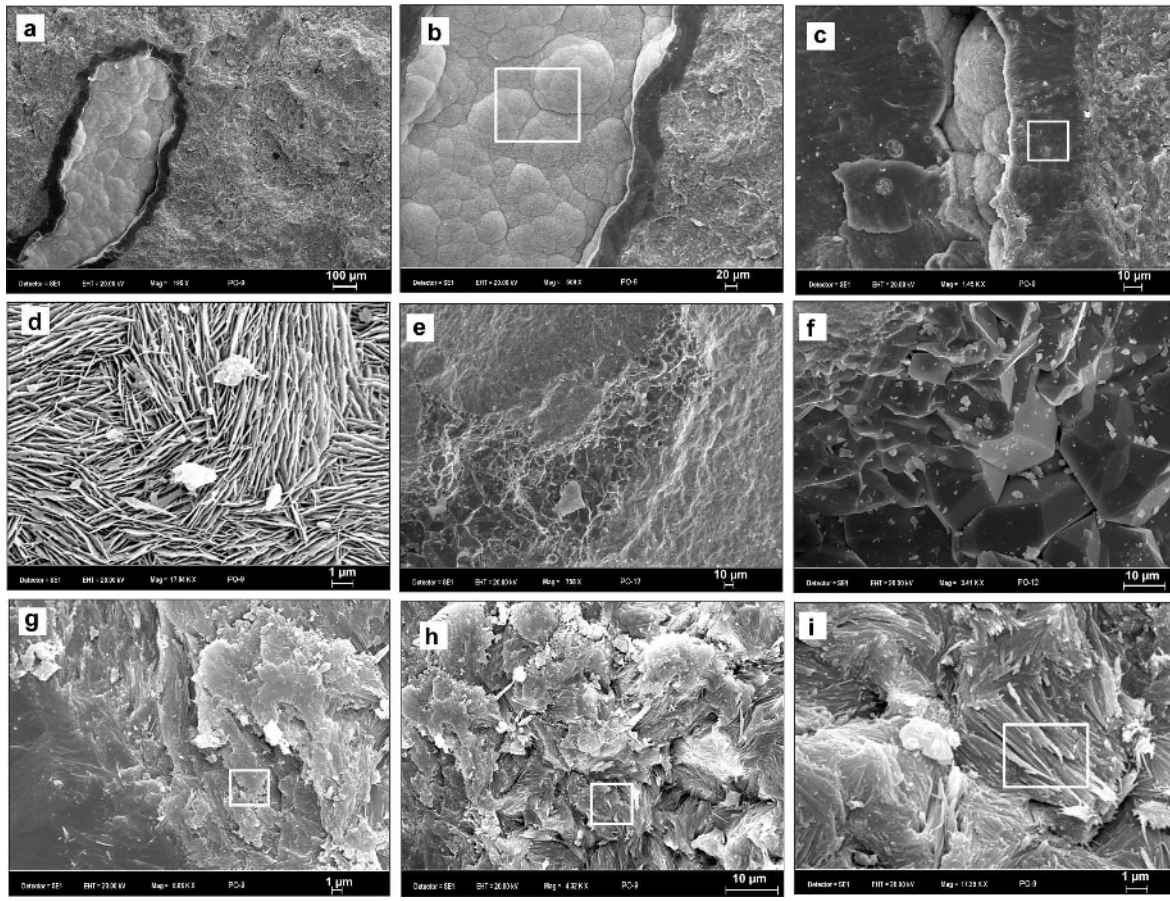

Figure 7. (a–c) Opal and quartz (chalcedony) were found in cavities of the sepiolitic claystone. The spherical particles of amorphous silica with a diameter of ~0.5–100 µm are tightly packed with botryoidal opal-A and opal-CT lepispheres. The lamellae containing crystalline silica generally display an amorphous rim with a diameter of 5–30 µm, and the crystalline area has a characteristically uniform contrast. (d) Aggregated small, hexagonal, blade-shaped quartz crystals are also seen. (e,f) Several platy silica particles show a continuous transition between amorphous silica (opal-A) and crystallized silica (opal-CT-quartz). The particles are composed of several closely stacked, thin lamellae, with pseudo-hexagonal shapes and diameters of 200–300 nm across. The opal-CT is converted to quartz. (g–i) In the globular grains, long, thin fibers of sepiolite show progressive transformation to short and thick (Mg-poor) sepiolite fibers to opal-CT to euhedral quartz.

an amorphous rim with a 5–30 µm diameter, and the crystalline area had a characteristically uniform contrast (Figure 7a–f). The increase in silica crystallinity was also confirmed by the textural and mineralogical changes seen in the SEM images. The dehydration of the opal-CT-associated cavity apparently increased as opal-CT was converted to quartz (Figure 7e,f). In the globular grains, long, thin fibers of sepiolite showed progressive transformation to short, thick (Mg-poor) sepiolite fibers, to opal-CT, to idiomorphic quartz (Figure 7g–i, Table 3). The Mg content of the thick, short fibers was less than that of the thin fibers and the Si contents were greater.

GEOCHEMISTRY

Dolostones, limestones, sepiolitic claystone, Mg-rich smectitic claystone chert, and detrital silicate-rich rock samples which were nearly pure were selected for chemical analysis. The major- and trace-element contents in the selected representative samples were compiled (Table 2) and the *REE*, TRE, HFSE, and LILE values of each group were evaluated. Groups were identified based on mineralogical and chemical analyses of samples very rich in each of these minerals, *e.g.* calcite, dolomite, sepiolite, Mg-smectite, *etc.* (Table 1). The major- and trace-element contents revealed clear differentiation based on the source. Significant positive correlations were found for Al, Fe, Ti, and K which were concentrated in the detrital silicate-rich rocks. Mg and Ca were mainly concentrated in neoformed minerals (sepiolitic claystone, Mg-rich smectitic claystone, dolostone, and calcite). Si and Na were found in both groups. The trace-element contents (*REE*, TRE, HFSE, and LILE) were observed to cluster in two groups. All *REE* in the sepiolitic claystone were strongly positively correlated with each other (r^2 >

https://doi.org/10.1346/CCMN.2011.0590306 Published online by Cambridge University Press

0.90) (Table 4, [available from the 'Deposited Material' section of journal pages on The Clay Minerals website: www.clays.org/journal/JournalDeposits.html]). The *REE* were positively correlated with Al_2O_3 and Fe_2O_3 (r^2 > 0.71) in dolostone and sepiolitic claystone, but were not correlated in limestone or in detrital silicate-rich rocks (Table 4). The *REE* were clearly concentrated in the detrital silicate-rich rocks (187 ppm) but were less prevalent (<5 ppm) in dolostone, limestone, and silica-rich rocks; the *REE* contents in sepiolitic claystone and Mg-rich smectitic claystone samples ranged from 4.30 to 13.5 and 75 ppm, respectively. The TRE (Co, Cr, Cu, Ni, V, Sc, and Zn; Jenner, 1996) contents were <35 ppm in limestone and dolostone, but were 114 ppm, 141 ppm, and 336 ppm in sepiolitic claystone, Mg-rich smectitic claystone, and detrital silicate-rich rocks, respectively (Table 2). The TRE were not correlated with *REE* elements in limestone, dolostone, and detrital silicate-rich rocks, but were moderately negatively correlated with sepiolitic claystone ($r^2 = -0.62$). They have a strong positive correlation with Mg-rich smectitic claystone (r^2 = 0.94). The HFSE (Hf, Nb, Ta, Th, Ti, and Zr, Saunders *et al*., 1980) contents were similar in dolostone, limestone, sepiolitic claystone, and Mg-rich smectitic claystone, but the HFSE content was >10 times greater in detrital silicate-rich rocks. The HFSE was negatively correlated with TRE ($r^2 > -0.72$) in Mg-rich smectitic claystone, and no correlation was found in other mineral groups. The *REE*, Al_2O_3, Fe_2O_3, K_2O, TiO_2, Zr, Th, and Y were strongly correlated with each other in dolostone, sepiolitic claystone, and Mg-rich smectitic claystone; in detrital silicate-rich rocks and limestone, no correlations were found. Moderate to strong negative correlations (r^2 = −0.89, −0.60, and −0.28) were found between Al_2O_3 and MgO in the dolostone, sepiolitic claystone, and limestone, respectively, except detrital silicate-rich rocks were weakly positive correlated (r^2 = 0.43; Table 4). As would be expected, CaO contents were greater in limestone and in some dolostones, whereas MgO and SiO_2 were high in sepiolitic claystone and Mg-rich smectitic claystone, and SiO_2 was very high in siliceous beds and nodules. Al_2O_3 was sometimes >1% in Mg-rich smectitic claystone and basal sepiolites. Negative or no correlation was observed between SiO_2 and CaO in all sample groups. SiO_2 and MgO showed moderately positive and slightly positive correlations in sepiolitic claystone and detrital silicate-rich rocks, respectively. The *REE* showed strongly positive correlations with Al_2O_3, Fe_2O_3, TiO_2, Zr, and HFSE (r^2 = 0.71−0.98) in dolostone and sepiolitic claystone and a strongly to moderately negative correlation with MgO (r^2 = −0.93−0.58). The LILE (Ba, K, Rb, Sr, Th, U, Pb, La, and Ce; Schilling, 1973) contents were similar to those of dolostone, limestone, and sepiolitic claystone whereas the LILE content was 5−10 times greater in Mg-rich smectite and detrital silicate-rich rocks of the sample groups (Table 2).

No correlation was found between Ca and Sr in any rock groups, indicating that the distribution of Sr is not related to the Ca^{2+} content. The Ba and Sr were special cases because in carbonate rocks they normally appear at concentrations of <300 ppm. In some of the present samples their concentrations were high (up to 900 ppm). The Sr content was large in the limestone (1674 ppm), dolostone (1274 ppm), Mg-rich smectitic claystone (960 ppm), and detrital silicate-rich rocks (1271 ppm), and the smallest Ba content was found in sepiolite-rich claystones (380 ppm). The largest Ba contents were found in detrital, silicate-rich rocks (520 ppm) and Mg-rich smectitic claystones (420 ppm), while it was smallest in sepiolitic claystones (79 ppm). The average Ba contents of limestone and dolostone were 203 and 195 ppm, respectively. The greatest Sr content was determined in one of the dolostone samples which contained celestite ($SrSO_4$); the SrO content was 5.32%. Taking all samples into consideration, correlation between the two elements was not significant.

Most elements in the sepiolitic claystones investigated were present in smaller amounts than in the Eskişehir sepiolitic claystones (Table 5), but Ba, Sr, and TRE values were greater than for Spanish sepiolites (Çoban, 2001; Torres-Ruiz *et al*., 1994). Some of the *REE* contents of the Spanish sepiolites are greater than those of the Polatlı sepiolites; Eskişehir sepiolites are similar to those of Polatlı in terms of *REE* contents.

The MgO content of the <2 μm fraction of the sepiolite-rich claystones was 19.08−23.9%, and the SiO_2 content was 46.7−55.06% (Table 6). The MgO contents and SiO_2/MgO ratios of the Polatlı sepiolites ranged from 2.30 to 2.70, and these ratios are similar to natural sepiolite (Weaver, 1989). Many of the SiO_2/MgO ratios were greater than the natural ratio (2.23) of sepiolite (Weaver, 1989) because the average SiO_2 (54.13%) and MgO (21.96%) contents of the sepiolites are lower than the theoretical sepiolite compositions (SiO_2 = 55.66, MgO = 24.89). Using the Brauner-Preisinger model (Bailey, 1980), structural formulae were calculated for the clay fraction assuming homogeneous composition (Table 6). The average structural formulae of sepiolites was calculated on the basis of 32 oxygen atoms (Weaver and Pollard, 1973), giving a formula of $[Ca_{0.05}Na_{0.09}K_{0.05}(Si_{11.92}Al_{0.09})^{-0.09}(Mg_{7.41}Al_{0.31}Fe_{0.07}Ti_{0.01})^{-0.17}O_{30}(OH)_4 6H_2O]$. Little or no substitution of tetrahedral Al for Si (0.00−0.21) was observed. Mg was the dominant cation in the octahedral sheet, accompanied by minor amounts of Al, Fe, and rarely Ti. The chemical compositions of the <2 μm fraction of the purified Mg-rich smectite sample (Table 6) were used to calculate its half unit-cell formula (Weaver and Pollard, 1973), giving $[Ca_{0.11}Na_{0.02}K_{0.17}(Si_{3.84}Al_{0.16})(Mg_{1.81}Al_{0.54}Fe_{0.15}Ti_{0.01})^{-0.25}O_{10}(OH)_2]$. The tetrahedral Si was substituted by small amounts of Al. The number of octahedral cations, mostly Mg with minor amounts of Fe and A1, confirmed the trioctahedral character of the mineral.

https://doi.org/10.1346/CCMN.2011.0590306 Published online by Cambridge University Press

https://doi.org/10.1346/CCMN.2011.0590306 Published online by Cambridge University Press

Table 2. Major (wt.%) and trace elements (ppm) and some element ratios of dolostone, limestone, sepiolitic and Mg-rich smectitic claystone, and silica-rich and detrital silicate-rich rocks.

Element	Dolostone																
	I1-8/1	I1-8/2	I2-4	I3-32	I3-34	I4-0	I4-1	I4-8	I4-14	I5-16	I5-20	I7-11	I9-6	Max.	Min.	Mean	STDE
SiO_2	3.00	3.06	1.7	4.14	1.76	2.34	2.71	3.56	3.82	3.65	4.19	3.48	3.38	4.19	1.70	3.14	0.82
Al_2O_3	0.38	0.42	0.22	0.85	0.17	0.1	0.16	0.35	0.36	0.45	0.47	0.13	0.3	0.85	0.10	0.34	0.20
Fe_2O_3	0.18	0.24	0.09	0.32	0.04	0.04	0.09	0.14	0.14	0.17	0.56	0.07	0.18	0.56	0.04	0.17	0.14
MgO	18.81	18.64	19.88	16.32	19.11	19.4	20.01	19.86	19.3	18.57	18.22	20.06	19.68	20.06	16.32	19.07	1.02
CaO	31.19	31.23	31.43	32.78	32.14	32.1	31.04	30.51	30.57	30.58	30.35	29.62	29.97	32.78	29.62	31.04	0.91
Na_2O	0.15	0.15	0.09	0.16	0.15	0.15	0.13	0.12	0.15	0.1	0.14	0.08	0.09	0.16	0.08	0.13	0.03
K_2O	0.09	0.08	0.06	0.2	0.07	0.04	0.04	0.07	0.07	0.07	0.11	0.04	0.06	0.20	0.04	0.08	0.04
TiO_2	0.02	0.02	0.01	0.04	0.01	0.01	0.01	0.02	0.02	0.03	0.02	0.01	0.02	0.04	0.01	0.02	0.01
P_2O_5	0.01	0.01	0.01	0.07	0.04	0.03	0.02	0.01	0.01	0.02	0.06	0.02	0.03	0.07	0.01	0.03	0.02
Cr_2O_3	0.001	0.001	0.002	0.002	0.001	0	0.001	0.001	0.001	0.001	0.002	0.004	0.003	0.00	0.001	0.002	0.00
LOI	46.0	46.0	46.4	44.9	46.3	45.7	45.6	45.3	45.4	45.8	45.7	46.3	46.1	46.40	44.90	45.81	0.44
TOT/C	12.25	11.88	12.35	12.57	13.3	12.8	12.98	12.06	12.42	12.42	12.03	11.81	11.89	13.30	11.81	12.36	0.45
TOT/S	0.10	0.08	0.03	0.07	0.18	0.11	0.12	0.04	0.13	0.06	0.07	0.02	0.08	0.18	0.02	0.08	0.04
SUM	99.83	99.85	99.90	99.78	99.79	99.90	99.81	99.95	99.85	99.45	99.85	99.81	99.81	99.95	99.45	99.81	0.12
Ba	221.4	217.6	114	94.2	111.8	144	538.6	75.1	89.5	395.2	341	123.3	62.8	538.6	62.80	194.5	145.8
Co	0.50	1.00	<0.5	0.90	1.10	0.60	0.70	0.50	0.70	0.50	2.20	0.50	0.50	2.20	0.50	0.81	0.49
Cs	3.10	3.10	2.50	3.50	1.00	0.50	1.10	2.90	2.40	6.20	3.50	2.80	1.50	6.20	0.50	2.62	1.46
Ga	0.70	0.70	<0.5	1.00	0.50	0.50	0.50	0.60	0.50	0.50	0.50	0.50	0.50	1.00	0.50	0.58	0.15
Hf	0.50	0.50	<0.5	0.50	0.50	0.50	0.50	0.50	0.50	0.50	0.50	0.50	0.50	0.50	0.50	0.5	0.0
Nb	0.50	0.60	<0.5	1.00	0.50	0.50	0.50	0.50	0.70	0.70	0.70	0.50	0.50	1.00	0.50	0.6	0.15
Rb	4.70	4.60	3.50	11.60	2.50	1.00	1.70	3.90	3.90	5.60	6.30	2.00	3.20	11.60	1.00	4.19	2.70
Sr	878	900	1156	1368	1314	380	804	702	950	4439	730	1444	1315	4439	380.0	1260	1005
Ta	0.10	0.10	<0.1	0.10	0.10	0.10	0.10	0.10	0.10	0.10	0.10	0.10	0.10	0.10	0.10	0.10	0.00
Th	0.50	0.20	<0.2	0.70	0.10	0.10	0.10	0.20	0.50	0.60	0.50	0.10	0.20	0.70	0.10	0.32	0.22
U	2.70	2.70	3.30	7.70	6.40	1.20	2.50	7.60	7.40	3.60	15.00	13.40	14.90	15.00	1.20	6.80	4.87
V	10.00	10.00	<5.0	17.00	15.00	5.00	5.00	12.00	10.00	16.00	39.00	39.00	22.00	39.00	5.00	16.67	11.51
Zr	5.00	6.20	2.50	9.60	2.40	1.20	1.20	4.40	4.00	5.70	6.60	1.70	4.30	9.60	1.20	4.22	2.45
Y	0.90	0.80	0.60	1.50	0.40	0.10	0.30	0.80	0.70	1.00	1.30	0.30	0.70	1.50	0.10	0.72	0.40
La	1.40	1.40	0.80	3.20	0.50	1.30	1.00	1.20	1.50	1.20	1.80	0.10	0.70	3.20	0.10	1.24	0.75
Ce	2.90	2.80	1.70	5.50	1.10	0.30	0.50	1.90	1.70	2.60	3.20	0.70	1.60	5.50	0.30	2.04	1.40
Pr	0.27	0.33	0.16	0.58	0.09	0.05	0.06	0.20	0.20	0.30	0.37	0.07	0.18	0.58	0.05	0.22	0.15
Nd	1.00	1.10	0.70	2.20	0.40	0.30	0.30	0.90	0.80	1.00	1.30	0.40	0.70	2.20	0.30	0.85	0.52
Sm	0.20	0.20	<0.1	0.60	0.10	0.05	0.06	0.10	0.13	0.24	0.26	0.05	0.11	0.60	0.05	0.18	0.15
Eu	0.06	0.05	0.05	0.07	0.05	0.02	0.02	0.07	0.02	0.05	0.04	0.02	0.02	0.07	0.02	0.04	0.02
Gd	0.21	0.19	<.05	0.34	0.05	0.05	0.07	0.18	0.15	0.20	0.27	0.06	0.17	0.34	0.05	0.16	0.09
Tb	0.02	0.04	0.03	0.05	0.03	0.01	0.01	0.02	0.02	0.03	0.04	0.01	0.02	0.05	0.01	0.03	0.01
Dy	0.13	0.25	<.05	0.32	0.08	0.05	0.06	0.10	0.12	0.18	0.20	0.05	0.13	0.32	0.05	0.14	0.08
Ho	0.05	0.05	<.05	0.05	0.05	0.02	0.02	0.05	0.02	0.03	0.03	0.02	0.02	0.05	0.02	0.03	0.01
Er	0.07	0.08	0.07	0.16	0.05	0.03	0.05	0.09	0.06	0.06	0.12	0.03	0.07	0.16	0.03	0.07	0.04
Tm	0.05	0.05	<.03	0.05	0.05	0.01	0.01	0.05	0.02	0.01	0.01	0.01	0.01	0.05	0.01	0.03	0.02

https://doi.org/10.1346/CCMN.2011.0590306 Published online by Cambridge University Press

Yb	0.09	0.17	<.05	0.15	0.05	0.05	0.05	0.05	0.08	0.10	0.10	0.05	0.05	0.17	0.05	0.08	0.04
Lu	0.01	0.02	0.01	0.02	0.01	0.01	0.01	0.02	0.01	0.01	0.02	0.01	0.02	0.02	0.01	0.01	0.01
Cu	0.90	0.80	0.30	4.00	1.20	2.30	3.30	0.90	2.30	1.10	9.80	0.20	1.00	9.80	0.20	2.16	2.56
Pb	0.50	0.50	0.30	1.60	0.60	2.00	2.00	0.50	2.10	0.60	1.30	0.10	0.40	2.10	0.10	0.96	0.73
Zn	3.00	3.00	2.00	6.00	2.00	4.00	3.00	3.00	4.00	3.00	5.00	1.00	3.00	6.00	1.00	3.23	1.30
Ni	2.20	2.40	1.70	5.70	2.90	0.90	2.00	2.20	3.10	3.80	10.70	3.00	3.40	10.70	0.90	3.38	2.49
As	15.80	14.50	5.40	13.40	9.40	0.70	1.10	11.30	4.90	3.70	6.00	0.50	5.20	15.80	0.50	7.07	5.30
Mg/Ca	0.509	0.504	0.534	0.420	0.502	0.510	0.544	0.549	0.533	0.512	0.507	0.571	0.554	0.57	0.42	0.52	0.04
Sr/Ca	0.004	0.004	0.005	0.006	0.006	0.002	0.004	0.003	0.004	0.020	0.003	0.007	0.006	0.02	0.00	0.01	0.00
HFSE	169.6	170.9	106.0	556.5	238.0	193.2	149.5	169.0	168.8	274.1	389.7	150.0	256.2	556.5	106.0	230.1	122.1
REE	6.37	6.56	3.52	13.07	2.43	2.2	2.17	4.88	4.75	6.01	7.76	1.47	3.33	13.07	1.47	4.96	3.14
LREE	5.57	5.63	3.36	12.08	2.09	1.95	1.86	4.2	4.2	5.1	6.67	1.27	3.0	12.08	1.27	4.38	2.86
MREE	0.67	0.78	0.08	1.06	0.23	0.2	0.24	0.52	0.46	0.73	0.84	0.21	0.47	1.06	0.08	0.50	0.30
HREE	0.13	0.15	0.08	1.06	0.16	0.05	0.07	0.16	0.09	0.18	0.25	0.05	0.15	1.06	0.05	0.20	0.27
LREE/HRE	42.8	37.5	42.0	11.4	5.9	39.0	26.6	26.3	46.7	28.3	26.7	25.4	20.0	46.67	5.92	29.12	12.25
TRE	24.44	25.04	18.68	48.28	30.04	20.64	21.84	20.34	27.94	32.24	81.39	72.07	49.03	81.39	18.68	36.3	20.5
LILE	1859	1794	1777	3153	2019	862	1683	1373	1637	5430	2013	1915	1897	5430	862.0	2109	1118
Eu*	1.38	1.21		0.73	3.33	1.88	1.45	2.46	0.67	1.07	0.71	1.72	0.69	3.33	0.67	1.44	0.81
Ce*	1.09	0.95	1.10	0.93	1.20	0.27	0.47	0.89	0.72	1.00	0.90	1.93	1.04	1.93	0.27	0.96	0.39
$(La/Lu)_N$	1.59	0.79	0.91	1.81	0.57	1.47	1.13	0.68	1.70	1.36	1.02	0.11	0.40	1.81	0.11	1.04	0.53

Table 2. (continued)

Element	Limestone															
	I3-3	I3-5	I3-8	I3-11	I3-25	I3-28	I3-31	I3-33	I3-34	I3-38	I6-1	I9-16	Max.	Min	Mean	STDE
SiO_2	3.13	2.94	1.12	2.82	3.27	3.60	1.76	4.15	1.55	1.75	3.24	1.82	4.15	1.12	2.60	0.96
Al_2O_3	0.76	0.61	0.14	0.49	0.41	0.34	0.3	0.52	0.17	0.29	0.8	0.32	0.80	0.14	0.43	0.21
Fe_2O_3	0.37	0.33	0.04	0.46	0.17	0.11	0.21	0.25	0.13	0.16	0.44	0.13	0.46	0.04	0.23	0.14
MgO	1.47	1.76	1.88	3.03	3.38	7.88	2.17	2.36	3.48	4.36	1.4	1.84	7.88	1.40	2.92	1.81
CaO	50.67	50.48	52.03	47.06	48.73	42.1	51.14	49.42	50.82	48.23	51.09	51.36	52.03	42.05	49.42	2.74
Na_2O	0.14	0.13	0.13	0.57	0.13	0.73	0.15	0.16	0.04	0.13	0.04	0.06	0.73	0.04	0.20	0.22
K_2O	0.22	0.18	0.05	0.18	0.1	0.17	0.07	0.15	0.05	0.1	0.16	0.07	0.22	0.05	0.13	0.06
TiO_2	0.04	0.03	0.01	0.03	0.02	0.02	0.02	0.03	0.01	0.02	0.08	0.01	0.08	0.01	0.03	0.02
P_2O_5	0.03	0.03	0.02	0.03	0.02	0.04	0.05	0.04	0.03	0.06	0.02	0.03	0.06	0.02	0.03	0.01
Cr_2O_3	0.005	0.004	0.003	0.008	0.002	0	0.001	0.001	0.001	0.001	0.001	0.001	0.01	0.00	0.00	0.00
LOI	42.9	43.2	44.3	45	43.4	44.8	43.9	42.7	43.5	44.7	42.5	44.1	45.00	42.50	43.75	0.85
TOT/C	10.7	12.26	12.78	12.16	12.68	8.24	12.26	11.56	12.13	12.25	12.05	11.81	12.78	8.24	11.74	1.23
TOT/S	0.05	0.06	0.11	0.12	0.14	0.04	0.12	0.12	0.03	0.04	0.01	0.08	0.14	0.01	0.08	0.04
SUM	99.75	99.71	99.74	99.69	99.64	99.8	99.78	99.78	99.79	99.8	99.8	99.75	99.80	99.64	99.75	0.05
Ba	233.6	178.3	311.1	285.9	303.3	319.1	311.0	214.8	59.9	155.2	63.8	184.5	319.1	59.9	218.4	93.0
Co	1.2	1.4	0.7	4.1	0.5	1.3	2.7	1.3	0.7	2.0	2.4	0.7	4.1	0.5	1.6	1.1
Cs	3.1	2.1	0.9	2.9	2.3	4.8	1.6	2.2	1.1	1.5	2.6	1.3	4.80	0.90	2.20	1.08
Ga	1.2	0.7	0.5	0.5	0.5	1.6	0.5	0.5	0.5	0.5	1.3	0.5	1.60	0.50	0.73	0.40

https://doi.org/10.1346/CCMN.2011.0590306 Published online by Cambridge University Press

Element	Limestone															
	I3-3	I3-5	I3-8	I3-11	I3-25	I3-28	I3-31	I3-33	I3-34	I3-38	I6-1	I9-16	Max.	Min	Mean	STDE
Nb	1.1	0.8	0.5	0.8	0.5	1.4	0.5	0.8	0.5	0.5	1.6	0.5	1.60	0.50	0.79	0.38
Rb	12.1	10	2.1	5.9	4.7	17.2	3.2	7.4	2.2	4.2	8.9	4.2	17.20	2.10	6.84	4.53
Sr	1544	1888	1727	2235	2376	1405	1061	2049	1304	1369	1267	1861	2376	1061	1673.8	414.8
Ta	0.1	0.1	0.1	0.1	0.1	0.1	0.1	0.1	0.1	0.1	<0.1	0.1	0.10	0.10	0.10	0.00
Th	1.2	1.1	0.2	0.7	0.3	2	0.2	0.8	0.4	0.3	1.2	0.6	2.00	0.20	0.75	0.54
U	3.7	3.3	9.7	4.6	13.1	3.4	11.3	2.5	3.8	4.4	0.8	3.0	13.10	0.80	5.30	3.85
V	24	20	15	48	20	18	15	5.0	5.0	6.0	18	6.0	48.00	5.00	16.67	11.93
Zr	9.6	8.0	2.1	8	4.7	12.1	4.5	6.3	2.4	4	18.6	3.7	18.60	2.10	7.00	4.73
Y	1.7	1.6	0.3	1.0	0.7	2.2	0.6	0.9	0.4	0.6	2.1	0.6	2.20	0.30	1.06	0.67
La	4.0	2.6	1.1	1.7	1.6	4.9	1.4	2.2	0.9	1.4	3.8	0.5	4.90	0.50	2.18	1.38
Ce	6.1	4.6	1.1	3	2.4	9.1	1.8	3.2	0.8	1.7	5.9	1.7	9.10	0.80	3.45	2.51
Pr	0.67	0.51	0.09	0.31	0.28	0.92	0.2	0.39	0.1	0.2	0.66	0.21	0.92	0.09	0.38	0.26
Nd	2.2	1.7	0.6	0.8	0.9	3.7	0.9	1.3	0.4	0.8	2.3	0.9	3.70	0.40	1.38	0.95
Sm	0.3	0.4	0.1	0.2	0.3	0.6	0.1	0.28	0.08	0.09	0.5	0.09	0.60	0.08	0.25	0.18
Eu	0.08	0.05	0.05	0.05	0.05	0.11	0.05	0.04	0.02	0.03	0.1	0.09	0.11	0.02	0.06	0.03
Gd	0.25	0.35	0.09	0.27	0.27	0.42	0.13	0.25	0.09	0.11	0.42	0.09	0.42	0.09	0.23	0.13
Tb	0.06	0.04	0.01	0.05	0.02	0.08	0.02	0.04	0.01	0.02	0.07	0.02	0.08	0.01	0.04	0.02
Dy	0.27	0.23	0.05	0.14	0.13	0.34	0.08	0.19	0.05	0.13	0.35	0.11	0.35	0.05	0.17	0.10
Ho	0.07	0.06	0.05	0.05	0.05	0.06	0.05	0.04	0.02	0.03	0.07	<0.02	0.07	0.02	0.05	0.02
Er	0.14	0.14	0.05	0.09	0.09	0.21	0.06	0.08	0.03	0.06	0.24	0.03	0.24	0.03	0.10	0.07
Tm	0.05	0.05	0.05	0.05	0.05	0.05	0.05	0.01	0.01	0.01	0.03	0.01	0.05	0.01	0.04	0.02
Yb	0.13	0.09	0.05	0.05	0.09	0.23	0.06	0.09	0.06	0.08	0.18	<0.05	0.23	0.05	0.10	0.06
Lu	0.03	0.03	0.01	0.02	0.02	0.03	0.01	0.01	0.01	0.01	0.04	0.01	0.04	0.01	0.02	0.01
Cu	3.1	3.3	3.7	9.5	2.2	9.6	10.8	6.4	3.3	8.7	68.4	2.9	68.40	2.20	10.99	18.35
Pb	1.8	1.9	0.4	1.0	0.5	4.4	4.0	1.8	1.1	1.7	1.8	0.7	4.40	0.40	1.76	1.26
Zn	3.0	2.0	1.0	4.0	2.0	18.0	17.0	4.0	3.0	4.0	1.3	3.0	18.00	1.00	5.19	5.84
Ni	3.0	3.4	2.1	17.9	2.8	24.2	26.1	2.6	3.2	3.7	3	2.6	26.10	2.10	7.88	9.15
As	4.2	4.9	12.3	19.1	11	6.2	8.2	4.2	2.0	2.6	9.1	5.9	19.10	2.00	7.48	4.86
Mg/Ca	0.02	0.03	0.03	0.05	0.06	0.16	0.04	0.04	0.06	0.08	0.00	0.55	0.55	0.00	0.09	0.15
Sr/Ca	0.00	0.01	0.00	0.01	0.01	0.00	0.00	0.01	0.00	0.00	0.00	0.01	0.01	0.00	0.00	0.00
HFSE	382	320	150	320	213	309	344	362	194	387	587	256	587.1	150.4	318.7	113.7
REE	14.35	10.85	3.4	6.78	6.25	20.8	4.91	8.12	2.58	4.67	14.66	3.33	20.8	2.6	8.4	5.6
LREE	13.0	9.4	2.9	5.8	5.2	18.6	4.3	7.1	2.2	4.1	12.7	3.0	18.6	2.2	7.4	5.1
MREE	1.0	1.1	0.4	0.8	0.8	1.6	0.4	0.8	0.3	0.4	1.5	0.5	1.6	0.27	0.80	0.45
HREE	0.4	0.3	0.2	0.2	0.3	0.5	0.2	0.2	0.1	0.2	0.5	0.2	0.5	0.11	0.26	0.13
LREE/HREE	37.1	30.4	18.1	27.7	20.7	35.8	23.9	37.3	20.0	25.6	25.8	20.0	37.3	18.1	26.9	6.9
TRE	69.5	58.5	44.0	139.2	42.2	78.9	79.4	27.1	23.0	32.2	96.4	49.0	139.2	23.0	61.6	33.5
LILE	3633	3584	2468	4032	3532	3176	1975	3526	1788	2368	2681	1897	4032	1788	2888	784.4
Eu*	1.38	0.63	2.48	1.01	0.83	1.03	2.06	0.71	1.11	1.42	1.03	0.69	2.48	0.63	1.20	0.57
Ce*	0.86	0.92	0.81	0.95	0.83	0.99	0.78	0.80	0.62	0.74	0.86	1.04	1.04	0.62	0.85	0.12
$(La/Lu)_N$	1.51	0.98	1.25	0.96	0.91	1.85	1.59	2.49	1.02	1.59	1.08	0.40	2.49	0.40	1.30	0.54

Table 2. (continued).

https://doi.org/10.1346/CCMN.2011.0590306 Published online by Cambridge University Press

Element	Sepiolitic claystone																
	I4-5	I4-6	I7-2	I7-4	I7-5	I7-9	I7-13	I7-19	I9-1	I9-4	PO-1	PO-3	PO-4	Max.	Min.	Mean	STDE
SiO_2	45.19	47.48	49.78	50.76	51.15	43.5	51.52	51.2	50.09	46.56	46.72	53.62	55.13	55.1	43.45	49.43	3.37
Al_2O_3	2.43	1.68	1.32	0.49	0.38	0.43	0.44	0.48	0.69	0.76	2.55	2.88	0.41	2.88	0.38	1.15	0.93
Fe_2O_3	1.03	0.72	0.55	0.21	0.13	0.16	0.14	0.21	0.31	0.23	1.05	1.16	0.22	1.16	0.13	0.47	0.39
MgO	20.36	21.34	21.3	23.04	22.54	21.4	21.5	22.6	22.11	20.1	19.08	19.42	23.5	23.5	19.08	21.41	1.37
CaO	6.24	5.08	3.76	2.62	2.47	2.91	3.20	2.60	3.14	2.30	5.48	1.75	0.46	6.24	0.46	3.23	1.58
Na_2O	0.13	0.09	0.05	0.03	0.02	0.07	0.07	0.02	0.08	0.06	0.10	0.10	0.01	0.13	0.01	0.06	0.04
K_2O	0.46	0.34	0.25	0.1	0.08	0.09	0.09	0.09	0.23	0.17	0.42	0.48	0.09	0.48	0.08	0.22	0.15
TiO_2	0.14	0.10	0.07	0.03	0.02	0.02	0.02	0.03	0.04	0.04	0.14	0.16	0.02	0.16	0.02	0.06	0.05
P_2O_5	0.02	0.02	0.01	0.01	0.02	0.03	0.02	0.01	0.03	0.03	0.01	0.02	0.006	0.03	0.006	0.02	0.01
Cr_2O_3	0.004	0.002	0.004	0.009	0.004	0.01	0.003	0.003	0.003	0.003	0.004	0.004	0.001	0.01	0.001	0.00	0.00
MnO	0.02	0.03	0.01	0.01	0.02	0.03	0.02	0.01	0.03	0.03	0.01	0.02	0.01	0.03	0.01	0.02	0.01
LOI	24.0	23.2	22.8	22.6	23.1	23.4	23.0	22.8	23.2	20.0	23.9	20.0	19.8	23.9	19.8	22.45	1.49
TOT/C	2.56	2.01	1.76	1.23	0.97	5.43	5.69	0.66	1.75	4.95	2.57	1.22	0.36	5.69	0.36	2.40	1.82
TOT/S	0.03	0.02	0.06	0.01	0.02	0.02	0.08	0.01	0.09	0.04	<0.02	<0.02	<0.02	0.09	0.01	0.04	0.03
SUM	100.0	100.0	99.91	99.91	99.91	100.0	100.0	99.93	99.93	99.86	99.51	99.58	99.58	100.0	99.51	99.86	0.18
Ba	101.6	83.0	53.8	37.6	33.2	43.8	116.5	20.8	17.7	42.9	231.0	174	17.0	231.0	17.0	74.8	65.71
Co	2.10	2.40	2.10	1.60	1.00	0.70	0.60	0.90	1.10	0.60	3.30	3.10	0.70	3.30	0.60	1.55	0.96
Cs	32.70	24.00	17.20	7.50	6.60	7.90	5.30	8.50	7.90	12.90	29.00	39.30	5.90	39.3	5.30	15.75	11.65
Ga	3.10	2.30	1.90	0.90	0.60	0.70	0.50	0.70	0.70	1.00	3.20	3.40	0.70	3.40	0.50	1.52	1.11
Hf	0.90	0.70	0.50	0.50	0.50	0.50	0.50	0.50	0.50	0.50	1.00	1.00	0.20	1.00	0.20	0.60	0.23
Nb	2.70	2.00	1.80	1.50	0.60	0.70	0.70	0.50	1.10	1.20	3.60	4.00	0.60	4.00	0.50	1.62	1.17
Rb	40.90	26.40	24.50	7.40	6.00	6.50	5.60	6.20	9.30	14.30	39.40	42.50	6.90	42.5	5.60	18.15	14.69
Sr	245.9	196.9	373.6	348.6	297.8	210	227.7	55.5	249.7	654.2	1126	571.1	90.9	1126	55.5	357.5	285.6
Ta	0.20	0.10	0.10	0.10	0.10	0.10	0.10	0.10	0.10	0.10	0.20	0.30	0.10	0.30	0.10	0.13	0.06
Th	2.10	1.40	0.80	1.20	0.20	0.30	0.40	0.20	0.70	0.90	2.60	2.60	0.40	2.60	0.20	1.06	0.87
U	3.20	3.30	0.60	0.90	0.40	2.40	2.70	0.80	5.90	10.60	1.40	0.80	0.30	10.6	0.30	2.56	2.90
V	29.0	33.0	57.0	71.0	59.0	102.0	40.0	107.0	86.0	84.0	70.0	49.0	240.0	240.0	29.0	79.0	54.29
Zr	27.5	19.0	16.6	9.20	4.70	5.20	6.30	7.50	9.00	9.10	32.0	35.6	6.10	35.6	4.70	14.4	10.81
Y	5.10	3.40	1.60	1.00	0.60	0.70	0.80	0.50	1.10	1.30	3.70	3.90	0.50	5.10	0.50	1.86	1.58
La	6.20	4.50	2.00	2.00	0.40	0.90	0.80	0.60	1.90	1.40	5.50	5.40	0.80	6.20	0.40	2.49	2.11
Ce	13.60	10.40	4.50	2.70	1.50	2.10	2.00	1.60	3.30	4.00	11.90	11.30	1.40	13.6	1.40	5.41	4.58
Pr	1.48	1.08	0.54	0.28	0.20	0.25	0.23	0.18	0.38	0.44	1.39	1.44	0.18	1.48	0.18	0.62	0.52
Nd	5.70	4.00	1.80	1.00	0.80	1.00	1.20	0.90	1.80	1.80	5.10	5.30	0.70	5.70	0.70	2.39	1.90
Sm	1.20	0.80	0.32	0.17	0.17	0.17	0.09	0.10	0.31	0.33	0.95	1.05	0.12	1.20	0.09	0.44	0.40
Eu	0.24	0.19	0.10	0.09	0.06	0.05	0.03	0.02	0.06	0.04	0.20	0.22	0.03	0.24	0.02	0.10	0.08
Gd	0.85	0.66	0.32	0.23	0.14	0.17	0.16	0.12	0.28	0.32	0.76	0.84	0.11	0.85	0.11	0.38	0.29
Tb	0.17	0.09	0.05	0.06	0.02	0.03	0.02	0.02	0.05	0.05	0.13	0.15	0.02	0.17	0.02	0.07	0.05
Dy	0.80	0.62	0.29	0.20	0.08	0.13	0.15	0.05	0.20	0.26	0.71	0.75	0.08	0.80	0.05	0.33	0.28
Ho	0.15	0.15	0.05	0.07	0.02	0.03	0.03	0.02	0.04	0.04	0.13	0.14	0.01	0.15	0.01	0.07	0.05
Er	0.54	0.34	0.19	0.1	0.06	0.06	0.10	0.04	0.08	0.10	0.36	0.42	0.05	0.54	0.04	0.19	0.17
Tm	0.07	0.06	0.04	0.04	0.01	0.01	0.01	0.01	0.01	0.02	0.06	0.07	0.01	0.07	0.01	0.03	0.03
Yb	0.46	0.34	0.2	0.14	0.06	0.10	0.08	0.05	0.1	0.11	0.37	0.42	0.05	0.46	0.05	0.19	0.15

https://doi.org/10.1346/CCMN.2011.0590306 Published online by Cambridge University Press

Element	Sepiolitic claystone																
	I4-5	I4-6	I7-2	I7-4	I7-5	I7-9	I7-13	I7-19	I9-1	I9-4	PO-1	PO-3	PO-4	Max.	Min.	Mean	STDE
Lu	0.06	0.05	0.03	0.06	0.01	0.01	0.01	0.01	0.02	0.03	0.06	0.07	0.005	0.07	0.01	0.03	0.02
Cu	2.10	3.20	2.30	3.70	3.80	1.50	1.50	3.40	1.70	3.20	3.20	3.20	2.20	3.80	1.50	2.69	0.83
Pb	0.80	0.50	0.90	0.50	0.50	0.50	0.40	0.40	0.90	0.90	3.20	3.10	0.90	3.20	0.40	1.04	0.96
Zn	6.00	8.00	8.00	5.00	7.00	5.00	3.00	3.00	7.00	6.00	14.00	16.0	5.00	16.0	3.00	7.15	3.85
Ni	5.40	6.10	13.40	6.00	6.00	4.80	6.60	7.80	5.30	5.90	24.70	19.3	6.10	24.7	4.80	9.03	6.24
As	4.20	5.30	1.10	1.00	1.10	0.60	5.20	1.20	3.80	5.70	2.10	1.50	2.30	5.70	0.60	2.70	1.87
Mg/Ca	2.75	3.54	4.78	7.42	7.70	6.22	5.67	7.33	5.95	7.37	2.94	9.37	43.12	43.1	2.75	8.78	10.51
Sr/Ca	0.01	0.01	0.01	0.02	0.02	0.01	0.01	0.00	0.01	0.04	0.03	0.05	0.03	0.05	0.00	0.02	0.01
HFSE	146	709	482	235	213	257	215	232	381	382	920	1087	127	1087	127	414	306
REE	31.5	23.3	10.4	7.14	3.53	5.01	4.91	3.72	8.53	8.94	27.6	27.6	3.6	31.5	3.53	12.8	10.6
LREE	27.0	20.0	8.8	5.98	2.90	4.25	4.23	3.28	7.38	7.64	23.9	23.4	3.1	27.0	2.90	10.9	9.08
MREE	3.41	2.51	1.13	0.82	0.49	0.58	0.48	0.33	0.94	1.04	2.88	3.15	0.37	3.41	0.33	1.39	1.15
HREE	1.13	0.79	0.46	0.34	0.14	0.18	0.2	0.11	0.21	0.26	0.85	0.98	0.12	1.13	0.11	0.44	0.36
LREE/HREE	23.9	25.3	19.2	17.6	20.7	23.6	21.2	29.8	35.1	29.4	28.1	23.9	26.8	35.1	17.6	25.0	4.87
TRE	71.9	65.2	109	146.2	101.4	168.2	71.7	140	121	118	143	118	254	254	65.2	125	49.73
LILE	4233	3149	2536	1231	1004	1014	1103	833	2199	2141	4908	4795	866	4908	833	2309	1519
Eu*	1.12	1.23	1.47	2.14	1.83	1.38	1.18	0.86	0.96	0.58	1.11	1.10	1.23	2.14	0.58	1.25	0.40
Ce*	1.04	1.09	1.00	0.83	1.22	1.02	1.08	1.12	0.90	1.18	0.99	0.93	0.85	1.22	0.83	1.02	0.12
$(La/Lu)_N$	1.17	1.02	0.76	0.38	0.45	1.02	0.91	0.68	1.08	0.53	1.04	0.87	1.78	1.78	0.38	0.90	0.37

Table 2. (continued).

Element	Detrital silicate-rich rocks							Mg-rich smectitic claystone						
	PO-8	PO-9	PO-12	Max.	Min.	Mean	STDE	I11-17	I11-27	I11-37	Max.	Min.	Mean	STDE
SiO_2	77.52	79.87	92.29	92.29	77.52	83.23	7.94	50.83	49.96	51.01	51.01	49.96	50.60	0.56
Al_2O_3	0.26	0.17	0.08	0.26	0.08	0.17	0.09	12.39	3.62	7.54	12.39	3.62	7.85	4.39
Fe_2O_3	0.19	0.12	0.52	0.52	0.12	0.28	0.21	3.89	1.54	2.33	3.89	1.54	2.59	1.20
MgO	3.79	8.98	0.88	8.98	0.88	4.55	4.10	11.38	19.99	17.67	19.99	11.38	16.35	4.45
CaO	5.37	0.10	1.46	5.37	0.10	2.31	2.74	1.89	3.75	2.31	3.75	1.89	2.65	0.98
Na_2O	0.08	0.02	0.07	0.08	0.02	0.06	0.03	0.12	0.37	0.12	0.37	0.12	0.20	0.15
K_2O	0.06	0.04	0.04	0.06	0.04	0.05	0.01	3.06	0.70	1.71	3.06	0.70	1.82	1.19
TiO_2	0.01	<0.01	<0.01	0.01	0.01	0.01		0.30	0.22	0.19	0.30	0.19	0.24	0.06
P_2O_5	<0.01	<0.01	<0.01	0.00	0.00			0.03	0.08	0.03	0.08	0.03	0.05	0.03
Cr_2O_3	<0.002	<0.002	0.02	0.02	0.02	0.02		0.01	0.03	0.01	0.03	0.01	0.02	0.01
LOI	12.60	10.50	4.60	12.60	4.60	9.23	4.15	15.84	19.54	17.07	19.54	15.84	17.49	1.88
TOT/C	2.28	0.15	0.63	2.28	0.15	1.02	1.12	0.12	1.72	1.34	1.72	0.12	1.06	0.84
TOT/S	<0.02	<0.02	<0.02	0.00	0.00			0.01	0.05	0.03	0.05	0.01	0.03	0.02
SUM	99.89	99.83	99.96	99.96	99.83	99.89	0.07	99.88	99.80	99.99	99.99	99.80	99.89	0.10
Ba	123.0	50.0	164.0	164.0	50.0	112.3	57.7	264.0	247.4	749.7	749.7	247.4	420.4	285.3
Co	0.50	0.20	0.60	0.60	0.20	0.43	0.21	7.70	3.90	7.90	7.90	3.90	6.50	2.25

https://doi.org/10.1346/CCMN.2011.0590306 Published online by Cambridge University Press

Cs	2.10	2.00	0.30	2.10	0.30	1.47	1.01	143.3	47.1	86.0	143.3	47.1	92.1	48.4
Ga	<0.5	<0.5	<0.5	0.00	0.00			15.10	5.50	9.70	15.10	5.50	10.10	4.81
Hf	<0.10	<0.10	<0.10	0.00	0.00			3.40	1.50	2.40	3.40	1.50	2.43	0.95
Nb	0.40	0.30	0.10	0.40	0.10	0.27	0.15	21.60	5.80	14.00	21.60	5.80	13.80	7.90
Rb	2.90	2.60	0.80	2.90	0.80	2.10	1.14	261.1	49.1	129.2	261.1	49.1	146.5	107.0
Sr	258.3	30.6	56.9	258.3	30.6	115.3	124.6	975.0	1450.9	438.4	1450.9	438.4	954.8	506.6
Ta	<0.1	<0.1	<0.1	0.00	0.00			2.60	0.50	1.40	2.60	0.50	1.50	1.05
Th	0.20	<0.2	<0.2	0.20	0.20	0.20		22.90	4.30	15.30	22.90	4.30	14.17	9.35
U	12.50	25.20	2.30	25.20	2.30	13.33	11.47	5.80	5.10	2.10	5.80	2.10	4.33	1.97
V	8.00	29.00	<8.0	29.00	8.00	18.50	14.85	92.00	48.00	91.00	92.00	48.00	77.00	25.1
Zr	3.20	2.10	1.10	3.20	1.10	2.13	1.05	97.40	46.80	82.10	97.40	46.80	75.43	25.9
Y	0.40	0.20	0.20	0.40	0.20	0.27	0.12	15.00	8.30	9.70	15.00	8.30	11.00	3.53
La	0.60	0.20	0.20	0.60	0.20	0.33	0.23	21.90	9.80	15.70	21.90	9.80	15.80	6.05
Ce	1.20	0.40	0.40	1.20	0.40	0.67	0.46	42.70	21.00	32.80	42.70	21.00	32.17	10.8
Pr	0.14	0.06	0.04	0.14	0.04	0.08	0.05	4.48	2.27	3.50	4.48	2.27	3.42	1.11
Nd	0.60	<0.3	<0.3	0.60	0.60	0.60		16.60	9.30	13.00	16.60	9.30	12.97	3.65
Sm	0.10	<0.05	<0.05	0.10	0.10	0.10		3.50	1.90	2.60	3.50	1.90	2.67	0.80
Eu	0.02	<0.02	<0.02	0.02	0.02	0.02		0.45	0.33	0.39	0.45	0.33	0.39	0.06
Gd	0.09	<0.05	<0.05	0.09	0.09	0.09		2.72	1.48	2.06	2.72	1.48	2.09	0.62
Tb	0.02	<0.01	<0.01	0.02	0.02	0.02		0.48	0.22	0.34	0.48	0.22	0.35	0.13
Dy	0.07	<0.05	<0.05	0.07	0.07	0.07		2.50	1.45	1.91	2.50	1.45	1.95	0.53
Ho	<0.02	<0.02	<0.02	0.00	0.00			0.49	0.26	0.36	0.49	0.26	0.37	0.12
Er	0.03	<0.03	<0.03	0.03	0.03	0.03		1.47	0.82	1.08	1.47	0.82	1.12	0.33
Tm	<0.01	<0.01	<0.01	0.00	0.00			0.25	0.12	0.16	0.25	0.12	0.18	0.07
Yb	<0.05	<0.05	<0.05	0.00	0.00			1.65	0.82	1.17	1.65	0.82	1.21	0.42
Lu	<0.01	<0.01	<0.01	0.00	0.00			0.26	0.13	0.18	0.26	0.13	0.19	0.07
Cu	0.60	0.50	3.30	3.30	0.50	1.47	1.59	7.50	4.40	26.10	26.10	4.40	12.67	11.7
Pb	0.30	0.50	0.30	0.50	0.30	0.37	0.12	26.60	3.80	13.40	26.60	3.80	14.60	11.4
Zn	2.00	1.00	<1.0	2.00	1.00	1.50	0.71	52.00	20.00	35.00	52.00	20.00	35.67	16.0
Ni	1.90	2.40	4.30	4.30	1.90	2.87	1.27	67.80	27.20	64.60	67.80	27.20	53.20	22.5
As	3.70	1.20	6.80	6.80	1.20	3.90	2.81	4.10	4.80	5.10	5.10	4.10	4.67	0.51
Mg/Ca	0.60	75.77	0.51	75.77	0.51	25.62	43.43	14.44	6.77	16.45	16.45	6.77	12.55	5.11
Sr/Ca	0.01	0.04	0.01	0.04	0.01	0.02	0.02	0.20	0.08	0.07	0.20	0.07	0.12	0.07
HFSE	63.55	2.40	1.20	63.55	1.20	22.38	35.66	256.1	403.9	274.6	403.9	256.1	311.5	80.5
REE	3.24	0.66	0.64	3.24	0.64	1.51	1.50	99.5	49.9	75.3	99.5	49.9	74.9	24.8
LREE	2.54	0.66	0.64	2.54	0.64	1.28	1.09	85.7	42.4	65.0	85.7	42.4	64.4	21.7
MREE	0.30			0.30	0.30	0.30		10.14	5.64	7.66	10.14	5.64	7.81	2.25
HREE	0.03			0.03	0.03	0.03		3.63	1.89	2.59	3.63	1.89	2.70	0.88
LREE/HREE				0.00	0.00			23.60	22.42	25.10	25.10	22.42	23.71	1.34
TRE	13.0	33.1	165.6	165.6	13.0	70.6	82.9	175.0	86.1	160.5	175.0	86.1	140.5	47.7
LILE	897.1	441.6	557.0	897.1	441.6	631.9	236.8	27577	7682	15994	27577	7682	17084	9992
Eu*	0.99			0.99	0.99	0.99		0.69	0.93	0.79	0.93	0.69	0.80	0.12
Ce*	0.96			0.96	0.96	0.96		0.99	1.03	1.02	1.03	0.99	1.01	0.02
$(La/Lu)_N$								0.95	0.85	0.99	0.99	0.85	0.93	0.07

Table 2. (continued).

https://doi.org/10.1346/CCMN.2011.0590306 Published online by Cambridge University Press

Element	Detrital silicate-rich rocks																		
	I1-19	I1-23	I1-25	I3-14	I3-15	I3-18	I3-21	I3-22	I3-30	I4-27	I4-5	I5-21	I9-13	Max.	Min	Mean	STDE	STD	DL
SiO_2	51.56	42.69	37.27	38.29	39.38	39.09	42.55	47.35	45.45	47.86	48.5	45.84	51.87	51.9	37.3	44.4	5.0	5.2	0.01
Al_2O_3	17.53	12.1	11.39	11.9	10.34	12.16	13.37	14.99	14.38	15.7	14.6	13.49	15.39	17.5	10.3	13.6	2.0	2.2	0.01
Fe_2O_3	6.76	4.88	4.44	4.57	4.75	4.37	5.15	6.44	5.92	6.14	6.28	5.43	6.4	6.8	4.4	5.5	0.9	0.9	0.04
MgO	4.0	3.77	5.2	3.47	2.54	3.78	3.2	3.86	5.11	4.59	4.21	4.17	5.92	5.9	2.5	4.1	0.9	1.0	0.01
CaO	0.83	12.83	15.16	15.85	17.78	14.78	12.18	6.12	6.67	0.81	5.09	8.24	1.12	17.8	0.8	9.0	6.1	6.3	0.01
Na_2O	0.39	0.47	0.46	0.45	0.58	0.47	0.47	0.56	0.33	1.67	0.42	0.44	0.48	1.7	0.3	0.6	0.3	0.4	0.01
K_2O	3.86	2.95	2.71	3.09	2.56	2.85	3.22	3.44	4.01	3.33	3.35	3.03	3.36	4.0	2.6	3.2	0.4	0.5	0.01
TiO_2	0.65	0.57	0.52	0.56	0.56	0.53	0.65	0.68	0.59	0.61	0.68	0.66	0.76	0.8	0.5	0.6	0.1	0.1	0.01
P_2O_5	0.05	0.1	0.11	0.15	0.14	0.13	0.11	0.09	0.21	0.08	0.11	0.1	0.04	0.2	0.0	0.1	0.0	0.1	0.01
Cr_2O_3	0.01	0.01	0.01	0.01	0.01	0.01	0.01	0.02	0.01	0.02	0.02	0.02	0.02	0.0	0.0	0.0	0.0	0.0	0
LOI	14.3	19.5	22.5	21.3	21	20.9	18.7	16.1	16.9	19.1	16.6	18.3	14.6	22.5	14.3	18.4	2.6	2.8	0.1
TOT/C	0.2	2.97	4.04	3.88	4.07	3.49	2.92	1.59	1.54	0.4	1.42	2.12	0.37	4.1	0.2	2.2	1.4	1.5	0.01
TOT/S	0.01	0.33	0.03	0.03	0.04	0.19	0.04	0.02	0.03	0.71	0.04	0.03	0.02	0.7	0.0	0.1	0.2	0.2	0.02
SUM	99.97	99.93	99.81	99.69	99.68	99.1	99.67	99.7	99.62	99.95	99.9	99.76	100	100.0	99.1	99.8	0.2	0.3	
Ba	451	463	657	527	685	626	631	536	372	340	472	518	490	685	340	520	106	114	1
Co	11.7	11.9	13.4	9.7	8.4	9.1	10	23.2	16	16.3	18.2	14.7	16.8	23.2	8.4	13.8	4.3	4.7	0.2
Cs	49.2	30.5	32.8	36	30.2	41.1	36.8	41.2	47.9	36.8	41.3	46.1	50.1	50.1	30.2	40.0	6.9	7.1	0.1
Ga	22.7	15.3	14.7	15.4	12.6	16.7	16.9	18.8	18.4	20.2	18.9	17	20.3	22.7	12.6	17.5	2.7	3.1	0.5
Hf	5.10	4.20	3.80	4.20	4.60	3.80	4.30	4.20	3.60	4.10	4.50	4.40	5.10	5.1	3.6	4.3	0.5	0.5	0.10
Nb	19.8	15.3	15.0	16.0	14.9	15.0	17.3	18.5	15.7	18.9	20.4	18.5	22.9	22.9	14.9	17.6	2.5	2.7	0.10
Rb	226	144	142	163	129	162	166	184	248	193	193	176	200	248	129	179	34	37.3	0.10
Sr	817	1019	1697	1199	1019	5297	1191	1058	1403	210	577	613	424	5297	210	1271	1277	1556	0.5
Ta	1.7	1.3	1.1	1.4	1.2	1.3	1.3	1.5	1.4	1.3	1.4	1.3	1.6	1.7	1.1	1.4	0.2	0.2	0.1
Th	23.6	16.4	18.8	21.9	16.3	19.6	20.3	20.3	18.5	18.1	20.7	18.2	23.3	23.6	16.3	19.7	2.3	2.5	0.2
U	6.0	14.2	11.0	5.0	5.8	7.7	4.1	4.9	7.0	5.8	4.4	6.3	5.7	14.2	4.1	6.8	2.8	3.2	0.1
V	137.0	102.0	101.0	81.0	66.0	99.0	86.0	152.0	89.0	128.0	111.0	107.0	155.0	155.0	66.0	108.8	27.2	29.3	8.0
Zr	161.2	140.3	123.7	132.4	156.4	124.4	142.3	148.4	134.3	141.8	155	146.4	175.5	175.5	124	144.8	14.8	16.3	0.1
Y	18.0	19.4	19.3	20.1	21.5	17.4	22.1	23.0	19.1	18.6	24.0	23.5	14.0	24.0	14.0	20.0	2.8	3.1	0.1
La	48.3	37.5	40.1	44.8	41.7	41.7	43.9	46.4	43.1	40.3	45.3	40.7	32.8	48.3	32.8	42.0	4.0	4.6	0.1
Ce	95.3	75.9	81.7	89.3	82.1	81.3	91.7	95.2	84.6	76.0	88.3	80.8	75.0	95.3	75.0	84.4	7.0	7.3	0.1
Pr	10.1	8.2	8.3	9.0	8.8	9.0	9.6	10.2	9.2	9.5	10.5	9.6	7.7	10.5	7.7	9.2	0.8	0.9	0.02
Nd	36.5	29.4	30.4	32.6	31.0	30.8	34.2	36.9	31.0	35.8	38.3	33.8	26.5	38.3	26.5	32.9	3.4	3.7	0.3
Sm	6.7	5.2	5.6	6.0	5.6	5.6	6.6	7.2	6.0	5.89	6.59	6.13	4.25	7.2	4.3	6.0	0.8	0.9	0.05
Eu	1.3	1.23	1.14	1.32	1.17	1.08	1.29	1.4	1.17	1.21	1.41	1.32	0.88	1.4	0.9	1.2	0.1	0.2	0.02
Gd	4.29	4.05	4.26	4.46	4.28	4.19	4.48	5.08	3.84	4.15	4.93	4.67	3.01	5.1	3.0	4.3	0.5	0.6	0.05
Tb	0.65	0.63	0.64	0.73	0.76	0.64	0.78	0.82	0.67	0.71	0.8	0.8	0.51	0.8	0.5	0.7	0.1	0.1	0.01
Dy	3.42	3.71	3.63	3.7	3.85	3.34	4.07	4.26	3.73	3.46	3.95	3.89	2.73	4.3	2.7	3.7	0.4	0.4	0.05
Ho	0.6	0.66	0.61	0.72	0.74	0.62	0.83	0.85	0.7	0.63	0.79	0.77	0.48	0.9	0.5	0.7	0.1	0.1	0.02
Er	1.68	2.04	1.76	1.91	2.08	1.59	2.18	2.37	1.83	1.86	2.23	2.2	1.39	2.4	1.4	1.9	0.3	0.3	0.03
Tm	0.27	0.33	0.28	0.31	0.32	0.25	0.33	0.37	0.29	0.28	0.35	0.35	0.26	0.4	0.3	0.3	0.0	0.0	0.01
Yb	2.02	1.71	1.84	1.84	1.85	1.61	1.93	2.05	1.77	1.69	2.09	2.04	1.43	2.1	1.4	1.8	0.2	0.2	0.05

Lu	0.26	0.27	0.26	0.31	0.23	0.34	0.34	0.27	0.27	0.3	0.3	0.22	0.3	0.2	0.3	0.0	0.0	0.01				
Cu	23.9	43.2	17.9	16.6	14.1	21.4	20.8	32.9	26.8	37.7	15.1	21.2	25.3	43.2	14.1	24.4	8.8	9.6	0.1			
Pb	27.8	19	20.1	33.2	18.5	22.2	23.8	25.7	22.8	20.9	20.9	23.9	24.9	33.2	18.5	23.4	4.0	4.6	0.1			
Zn	64.0	50.0	47.0	52.0	40.0	52.0	53.0	61.0	62.0	53.0	51.0	51.0	67	67.0	40.0	54.1	7.5	8.3	1			
Ni	45.9	55	41.7	33.2	29.9	37.7	48.5	76	53.6	50.6	49.4	54	66.9	76.0	29.9	49.4	12.7	14.2	0.1			
As	33.1	126.9	35.5	7.6	40.7	18	18.3	86.7	20.7	13	11.9	18.5	11.8	126.9	7.6	34.1	34.8	39.6	1			
Mg/Ca	0.66	0.25	0.29	0.18	0.12	0.22	0.22	0.53	0.65	4.78	0.70	0.43	4.46	4.8	0.1	1.0	1.6					
Sr/Ca	0.14	0.01	0.02	0.01	0.01	0.05	0.01	0.02	0.03	0.04	0.02	0.01	0.05	0.1	0.0	0.0	0.0					
HFSE	4302	4014	3741	4165	4145	3889	4541	4641	4608	4172	4738	4564	4934	4934	3741	4343	357					
REE	209.3	169.1	178.7	193.9	181.5	179.3	199.0	210.0	185.3	180.0	205.8	187.4	155.7	210.0	156	187.3	16.0					
LREE	190.2	151.0	160.5	181.7	169.2	168.4	186.0	195.9	173.9	161.6	182.4	164.9	142.0	195.9	142	171.3	15.7					
MREE	17.0	15.5	15.9	12.5	11.8	11.5	13.2	14.5	11.7	16.1	18.5	17.6	11.9	18.5	11.5	14.4	2.5					
HREE	2.2	2.6	2.3	13.4	13.5	11.9	14.3	15.5	12.5	2.4	5.0	4.9	1.9	15.5	1.9	7.9	5.6					
LREE/HREE	86.0	57.2	69.8	13.6	12.5	14.1	13.0	12.6	13.9	67.0	36.7	33.7	75.9	86.0	12.5	38.9	28.3					
TRE	394	369	294	299	257	313	327	476	356	410	36.7	377	463	476	36.7	336	111					
LILE	33739	26279	25165	27735	23249	29917	28903	30528	35489	28549	361	26630	29244	35489	361	26599	8542					
Eu*	1.26	1.10	1.20	1.13	1.05	1.12	1.09	1.15	1.15	1.16	1.16	1.16	1.14	1.3	1.0	1.1	0.1					
Ce*	1.00	1.03	1.02	0.99	0.97	1.03	1.01	0.98	0.90	0.93	0.94	1.09	0.99	1.1	0.9	1.0	0.0					
$(La/Lu)_N$	2.11	1.57	1.75	1.95	1.52	2.06	1.46	1.55	1.81	1.69	1.71	1.54	1.69	2.1	1.5	1.7	0.2					

STD: standards for major and for trace and refractory elements are SO-18 and DS-7. respectively; DL: detection limit. STDE: standard deviation. Max: maximum. Min: minimum.

Potassium, Ca, and some Na occupied the interlayer space (Table 6). Most of the layer charge derived from octahedral rather than tetrahedral substitution. The layer charge of the Mg-rich smectite (average = 0.43) was between 0.2 and 0.6 meq/g; for this reason it was classified as smectite. Classification as either saponite or stevensite was considered, but discounted because comparisons with reported and theoretical structural formulae for these minerals (Weaver and Pollard, 1975; Nemecz, 1981; Weaver, 1989) revealed significant differences. Polatlı smectites were thus classified as Mg-rich smectite rather than as stevensite or (Mg-rich) saponite.

The Sr/Ca ratios of the limestone and dolostone were less than those of the other sample groups. The Mg/Ca ratios of the limestone samples were less than those of the other samples (Table 2). Both Sr/Ca and Mg/Ca in the sepiolitic claystones were similar to ratios of Messinian and Modern seawater while these ratios in the Mg-rich smectitic claystones were greater than those of the Messinian and Modern seawater (Figure 8).

The *REE* and some of the HFSE, TRE, and LILE were normalized to PAAS (Average Post-Archaean Australian Shale, McLennan, 1985). In general, all the sample groups presented a near horizontal *REE* curve, with strong depletion relative to PAAS in dolostone, limestone, sepiolitic claystone, and silica-rich rocks, and slight depletion in Mg-rich smectitic claystones. LREE to HREE enrichments were not found (1.14 < La/Lu >1.72) (Table 2). The detrital silicate-rich rock samples showed slight LREE enrichment (Figure 9a). The *REE* content varied from 0.02 to 0.07 times PAAS for dolostone, limestone, and sepiolitic claystone, from 0.37 to 0.48 times PAAS in Mg-rich smectitic claystone, and from 0.64 to 1.1 times PAAS in detrital silicate-rich

Figure 8. Mg/Ca *vs*. Sr/Ca ratios of investigated samples compared with Modern seawater (de Villiers, 1999), Messinian seawater (De Deckker *et al*., 1988), and Mean River (Blatt *et al*., 1972).

https://doi.org/10.1346/CCMN.2011.0590306 Published online by Cambridge University Press

Table 3. EDS analysis results (wt.%) of areas indicated in Figures 6 and 7.

Figure	6b	6c	6e	6h	6k
Element	Si = 59.37 Mg = 35.37 Al = 3.13 Ca = 1.60	Si = 62.82 Mg = 31.69 Al = 1.35 Ca = 4.14	Si = 54.13 Mg = 17.91 Al = 15.14 Ca = 2.94 K = 4.24 Fe = 5.63	Si = 5.66 Mg = 4.74 Ca = 89.60	Si = 68.46 Mg = 25.64 Al = 3.10 Ca = 2.22 K = 0.58
Figure	7b	7c	7g	7h	7i
Element	Si = 100.0	Si = 100.0	Si = 93.58 Mg = 6.42	Si = 90.45 Mg = 9.55	Si = 88.36 Mg = 11.64

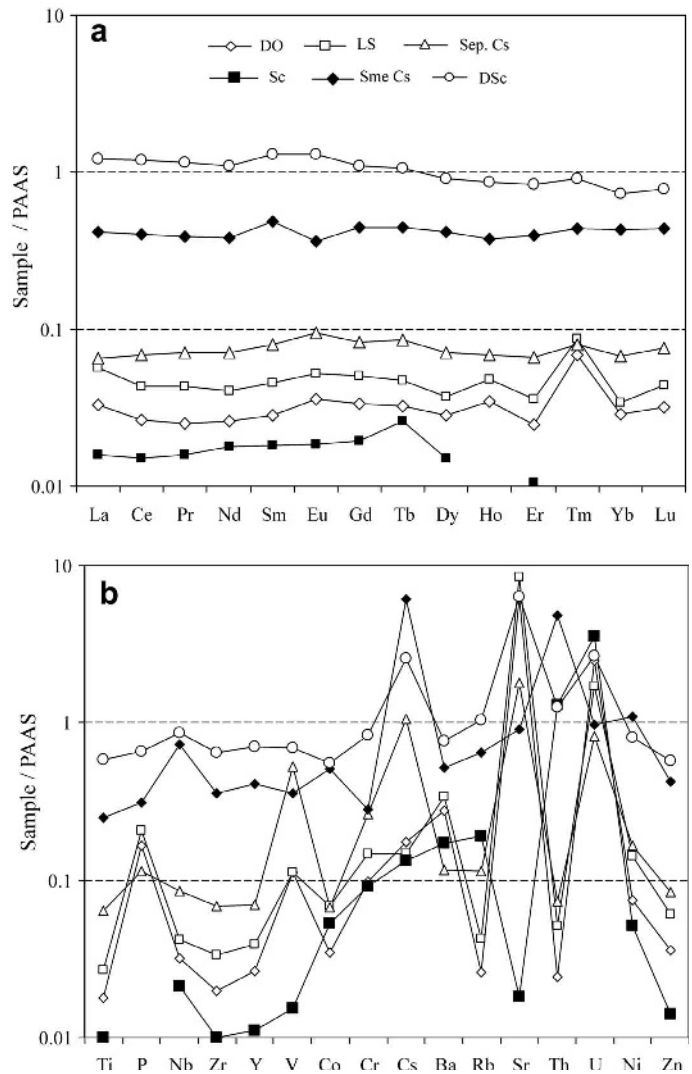

Figure 9. (a) PAAS-normalized *REE* pattern of the investigated sample groups (normalization values from Taylor and McLennan, 1985). (b) PAAS-normalized trace elements diagram of samples. The data are taken from Table 2. DO: dolostone, LS: limestone, Sep Cs: sepiolitic claystone, Sc: chert, Sme Cs: Mg-rich smectitic claystone, DSc: detrital silicate-rich rocks. Although clear depletion of the detrital silicate-rich rocks can be seen, similar and nearly parallel trends of the elements in the sample groups may be related to the similar origin of minerals.

https://doi.org/10.1346/CCMN.2011.0590306 Published online by Cambridge University Press

Table 5. Comparison of element contents of some sepiolites in the present study and from other studies.

Elements (ppm)	Spain* $n = 8$	Max./Min	STD	Eskişehir** $n = 6$	Max./Min	STD	This study $n = 13$	Max./Min	STD
Ba	27.13	55/<1	24.36	303.80	470/143	144.37	74.84	231/17	65.7
Sr	17.13	29/7	8.85	35852	58.390/8342	21.976.3	357.55	1.126/55	285.6
V	36.25	59/18	17.22	4457	5.716/3120	1835.7	79.0	240/29	54.3
TiO_2	0.045	0.11/0.03	0.03	0.04	0.05/0.02	0.015	0.06	0.16/0.02	0.06
MgO	23.88	26.53/20.19	2.06	24.69	25.87/23.86	0.70	21.78	23.5/19.08	1.37
MnO	0.018	0.02/0.01	0.008	0.02	0.03/0.01	0.008	0.02	0.03/0.01	0.01
REE	26.93	48.89/10.2	14.97	13.73	16.15/11.17	1.96	12.75	31.53/3.50	10.6
LREE	23.21	43.4/8.3	12.96	9.84	11.58/7.98	1.38	10.91	26.7/2.9	9.08
HREE	0.74	1.51/0.2	0.53	1.08	1.29/0.76	0.20	0.44	1.13/0.11	0.36
TRE	124.75	184/49	44.08	6801	11.302/3.317	3542	125.2	254/65.18	49.70

* Torres-Ruiz *et al*. (1994); ** Çoban (2001); STD: standard deviation.

Table 6. Chemical composition and structural formulae of sepiolites and Mg-rich smectites.

Samples	SiO_2	Al_2O_3	Fe_2O_3	MgO	CaO	Na_2O	K_2O	TiO_2	P_2O_5	Cr_2O_3	LOI	SUM
I4-5	55.06	2.51	1.17	20.42	0.09	0.27	0.4	0.12	0.03	0.004	19.80	99.88
I4-6	54.21	2.08	0.71	20.98	0.09	0.32	0.42	0.16	0.02	0.002	20.90	99.89
I7-2	55.02	2.01	0.19	22.16	0.11	0.24	0.30	0.11	0.01	0.004	20.09	100.24
I7-4	54.94	1.48	0.19	23.92	0.06	0.12	0.08	0.02	0.01	0.009	20.10	100.93
I7-5	54.95	1.36	0.10	22.98	0.1	0.17	0.05	0.02	0.02	0.004	19.97	99.72
I7-9	54.62	1.53	0.55	22.15	0.07	0.30	0.22	0.07	0.03	0.008	21.40	100.95
I7-13	54.77	1.64	0.27	22.32	0.17	0.17	0.11	0.04	0.02	0.003	20.50	100.01
I7-19	54.75	1.37	0.18	22.68	0.13	0.20	0.08	0.03	0.01	0.003	20.50	99.93
I9-1	55.08	1.13	0.26	22.89	0.11	0.26	0.12	0.04	0.03	0.003	20.60	100.52
I9-4	54.55	1.07	0.37	22.11	0.22	0.24	0.17	0.07	0.03	0.003	20.55	99.38
PO-3	46.72	2.55	1.05	19.08	5.48	0.10	0.42	0.14	0.01	0.004	23.90	99.45
PO-4	54.93	1.39	1.01	21.83	0.63	0.22	0.19	0.16	0.02	0.004	19.60	99.98
I10-17	51.97	12.67	3.98	11.64	0.68	0.21	3.13	0.31	0.03	0.011	15.30	99.93
I10-27	50.50	4.02	1.57	21.35	2.66	0.13	0.71	0.22	0.08	0.001	18.60	99.85
I10-37	55.13	0.60	0.28	23.57	0.36	0.12	0.09	0.02	0.01	0.001	19.80	99.98

Minerals	Sepiolites												– Mg-rich smectites –		
Samples	I4-5	I4-6	I7-2	I7-4	I7-5	I7-9	I7-13	I7-19	I9-1	I9-4	PO-3	PO-4	I10-17	I10-27	I10-37
Tetrahedral cations															
Si	11.94	11.92	11.89	11.79	11.92	11.92	11. 92	11.93	11.95	12.00	11.90	11.93	3.76	3.80	3.91
Al	0.06	0.08	0.11	0.21	0.08	0.08	0.08	0.07	0. 05	0.00	0.10	0.07	0.24	0.20	0.09
Octahedral cations															
Al	0.59	0.46	0.41	0.17	0.27	0.31	0.35	0.28	0.24	0.27	0.26	0.16	0.85	0.17	0.58
Mg	6.69	6. 97	7.75	7.75	7.53	7.30	7.34	7.46	7.50	7.35	7.14	7.70	1.27	2.43	1.78
Fe	0.19	0.12	0.03	0.03	0.02	0.09	0.05	0.03	0.04	0.06	0.17	0.05	0.22	0.09	0.14
Ti	0.02	0.03	0.02	0.03	0.00	0.01	0.00	0.00	0.01	0.01	0.03	0.00	0.02	0.01	0.01
OC	0.20	0.22	0.13	+0.11	0.06	0.14	0.11	0.10	0.14	0.26	0.34	0.18	0.19	0.33	0.23
Interlayer cations															
Ca	0.02	0.02	0.03	0.04	0. 02	0.02	0.04	0.03	0.03	0. 5	0.15	0.08	0.05	0.22	0.07
Na	0.12	0.14	0.11	0.05	0.07	0.13	0.07	0.09	0.11	0.10	0.09	0.05	0.03	0.02	0.02
K	0.11	0.12	0.08	0.02	0.01	0.06	0.04	0.02	0.01	0.05	0.05	0.03	0.29	0.07	0.16
ILC	0.27	0.30	0.24	0.15	0.12	0.23	0.19	0.17	0.19	0.25	0.44	0.24	0.42	0.52	0.32
TLC	0.26	0.30	0.24	0.32	0.13	0.22	0.19	0.17	0.19	0.26	0.44	0.25	0.43	0.53	0.32

Note: OC: octahedral sheet charge. ILC: interlayer charge. TLC: layer charge.

https://doi.org/10.1346/CCMN.2011.0590306 Published online by Cambridge University Press

rocks (Figure 9a). All sample groups had a positive Eu* anomaly, except Mg-rich smectitic claystone (0.80). Limestone, dolostone, and silica-rich samples showed a slightly negative Ce* anomaly while sepiolitic claystone and Mg-rich smectitic claystone samples had slightly positive anomalies (Table 2). The *REE* patterns of the detrital silicate-rich rocks were parallel to sepiolite-rich samples. In general, PAAS-normalized HFSE, TRE, and LILE patterns of the silica-rich rocks, dolostone, limestone, and sepiolitic claystone were similar, but depleted. The Mg-rich smectitic claystone and detrital silicate-rich rocks were only slightly depleted in HFSE and TRE, whereas LILE were enriched relative to PAAS (Figure 9b). The HFSE trend of Mg-rich smectitic claystones was similar to the detrital silicate-rich rock samples. The other neoformed mineral groups with relatively small HFSE contents also showed a concordant trend with each other.

DISCUSSION

The Polatlı basin represents an important Neogene lacustrine basin in central Anatolia. Sepiolitic claystone is alternated with dolostone beds at the bottom and especially middle levels of the sequence. The abundance of sepiolite in the succession decreases progressively toward the upper levels. Limestone becomes predominant in the same direction. The upper horizon generally comprises fossiliferous limestone, interfingered with gypsum beds. These lithological features are indicative of a past shallow and ephemerally hypersaline-evaporitic lake environment in the basin. In most cases, sepiolite formed in arid to semi-arid climates in closed terrestrial basins where it precipitated directly from Mg- and Si-enriched solutions with low Al concentrations (Mayayo *et al*., 1998).

The close relation between some of the fine-grained dolomite rhombs (<0.5 μm) and secondary coating or growth texture of dolomite and calcite minerals in the studied sample groups indicate secondary replacement or dissolution following precipitation of the primary minerals from the saturated lake water column in the Polatlı basin (Figure 6f–g) (indicated by arrow 2). Fine-grained (<3 μm) and euhedral to subhedral dolomite rhombs exhibited growth features. Growth of some of the sepiolite fiber bunches from the edges or faces of primary, fine-grained euhedral to subhedral dolomitic rhombs or as coatings on the dolomite indicates that these minerals were cogenetic. Sepiolite may have precipitated from Mg-rich solution as a consequence of dissolution of the dolomite. Filling of dissolution voids of euhedral to subhedral calcite crystals by sepiolite fibers also reveals that dissolution of calcite and precipitation of sepiolite occurred simultaneously.

The dolomites were deficient in Mg with a low Mg/Ca ratio (<0.55), fine-grain size (<0.5 μm), and euhedral to anhedral morphologies. These chemical and morphological properties are typical of primary or early diagenetic dolomites formed at low temperatures (Mayayo *et al*., 1996). The very low Sr/Ca ratio approximates the average of the representative river waters of the world (0.0027; Blatt *et al*., 1972). In the samples studied, the mean Mg/Ca mole ratios in limestone, dolostone, sepiolitic claystone, and Mg-rich smectitic claystone were 0.09, 0.52, 5.92, and 12.55, respectively, while the Sr/Ca mole ratio ranged from 0.02 to 0.002 in dolostone, 0.003 to 0.007 in limestone, 0.025 to 0.003 in sepiolitic claystone, and 0.20 to 0.074 in Mg-rich smectitic claystone (Table 2). Most oligo/mesohaline episodes known as the Messinian salinity crises were characterized by relatively high Sr/Ca (0.012–0.013) and Mg/Ca (2–3.6) ratios in waters in the Mediterranean region (Anadón *et al*., 2002). The variation of the Sr/Ca ratio was related to evaporation-dilution processes. Calcite was precipitated more from diluted lake water than the other minerals, especially Mg-rich smectite and partly sepiolite (Figure 8).

The clear differentiation of major and trace elements in the neoformed minerals (neoformed phyllosilicates, carbonates) and detrital silicate-rich rocks, and positive correlations between Al, Fe, Mn, K, Ti, and *REE* (both LREE and HREE), showed the different conditions for formation of the mineral groups. The strongly positive correlation between *REE* and Al_2O_3, Fe_2O_3, K_2O, TiO_2, Zr, Th, and Y indicated that the source of the *REE* was related to the detrital aluminosilicate fraction (*e.g.* micas, feldspars, *etc*.) dissolving after deposition (Table 3). The smaller *REE*, TRE, and HFSE contents of neoformed minerals than those of detrital silicate-rich rocks revealed that the minerals were precipitated directly in the basin because lake water is more dilute in terms of these elements.

The lack of or negative correlation between Ca and Sr in all neoformed mineral groups (Table 4) may be related to the addition of Sr from a different source, *e.g.* mineralized thermal water carrying anions and cations to the depositional basin along the fracture system, as revealed by several thermal springs in the basin. Kabata-Pendias and Pendias (2001) noted that the Sc content of mafic rocks (20–35 ppm) and of argillaceous sediments and shales (10–15 ppm) is relatively large, whereas in limestones and dolostones it is small (0.5–1.5 ppm). The Sc content in sepiolitic claystone, limestone, and dolostone was generally <1 ppm while the mean content of the element was 16 ppm in detrital silicate-rich rocks. The important differences between the element contents of neoformed and detrital minerals also indicated that the neoformed minerals precipitated directly from a lake-water column poor in this element.

Distribution of *REE* and the chemical composition found in the fibrous and detrital clays provided good clues as to the genesis of neoformed minerals. Indeed, most natural waters have extremely small *REE* contents (10^{-7}–10^{-2} ppm, McLennan, 1989), due to the fact that

https://doi.org/10.1346/CCMN.2011.0590306 Published online by Cambridge University Press

the fractionation and mobility of these elements is very unlikely between fluid and rock (Taylor and McLennan, 1985). The abundance of the elements in sediments was, therefore, clearly related to that of the parent rock from which they were derived (Bonnot-Courtois, 1981; Fleet, 1984). All sample groups had a positive Eu* anomaly, except Mg-rich smectite (0.80), when normalized to PAAS. Limestone, dolostone, and silica-rich rocks showed a slightly negative Ce* anomaly, while sepiolitic claystones, Mg-rich smectitic claystones, and detrital silicate-rich rocks had a slightly positive anomaly. Ce is fractionated from other *REE* due to the insolubility of Ce^{4+} under oxidizing environments (Braun *et al*., 1990; Class and la Roex, 2008). Enrichment of Ce^{4+} relative to other *REE* in slightly oxidizing conditions caused slight enrichment of Ce in Mg-rich smectitic claystones and detrital silicate-rich rocks. The oxidizing conditions also explain the negative Eu anomaly as it would have stabilized Eu^{3+} (Cullers *et al*., 1975). Europium can be divalent under reducing conditions. Some authors indicated that leaching of REE^{3+} is pH dependent; lower pH favors the mobility of REE^{3+} and higher pH can induce precipitation (Terkado and Fujitani, 1998; Moore, 1998; Aubert *et al*., 2001).

La and Th are more abundant in felsic than basic rocks, whereas Sc and Co are the opposite (Taylor and McLennan, 1985; Wronkiewicz and Condie, 1987). Ratios such as La/Sc, Th/Sc, Co/Th, Cr/Th, and Eu/Eu* in siliciclastic sediments allow constraints to be placed on the average provenance composition (*e.g.* Cullers, 1994, 1995; Cullers *et al*., 1988; Wronkiewicz and Condie, 1987, 1989, 1990; Cox *et al*., 1995). The La/Th ratio of the present samples, 2.5−5.08, was in the range of UCC (Upper Crust Composition, Taylor and McLennan, 1985), with most samples having a significant felsic component (2.5<La/Th<5.08). The La/Th ratio indicated that the sediments (average is 3.5) are similar to average upper crust composition (La/Th = 2.8). Thus, the concentrations of these elements and the corresponding elemental ratios in sediments may be useful for provenance determination. Scandium contents of <1.0 ppm indicated more felsic components. The Co/Th ratios of the samples were between 0.86 and 3.0, and thus close to UCC (0.93), NASC (Average North American Shale, Gromet *et al*., 1984) (2.09), and PAAS (1.58). These ratios indicate that the source of the samples was felsic rocks. The average Co content in ultramafic rocks is 105 ppm (Jagoutz *et al*., 1979), whereas Co in the present samples ranged from 0.50 to 3.30 ppm. The geochemical differences between elements such as Th and La (indicative of a felsic source) and Sc and Cr (indicative of a mafic source) have been exploited by various researchers to distinguish between felsic and mafic provenance (*e.g.* McLennan *et al*., 1980; McLennan, 1989; Wronkiewicz and Condie, 1990; McLennan and Taylor, 1991). The Th/Sc ratio (0.50−1.5) of the samples studied was related to the more felsic source rocks. The close similarity of the depleted *REE* trend of carbonates and sepiolitic claystone to each other and to detrital silicate-rich rocks may be related to a cogenetic source.

The content and correlation character of HFSE and TRE in carbonates and sepiolitic claystones indicated that precipitation of the minerals occurred under similar conditions. Because ophiolitic rocks are far from the drainage system of the study area, the element contents and ratios mentioned above represent source rocks from metamorphic, dolomitic metacarbonates, plutonic rocks, and especially volcanic rocks surrounding the immediate vicinity of the Polatlı area. The rocks might have served as sources for the Si and Mg required for sepiolite precipitation. For Spanish sediments, Torres-Ruíz *et al*. (1994) showed that carbonates, Mg-rich smectite claystones, and sepiolitic claystones had small *REE* contents (<20 ppm), which they interpreted as a clear sign of formation by direct precipitation from solution. The Eskişehir sepiolites were formed by the diagenetic replacement of magnesite pebbles with shallow burial under alkaline conditions in the vicinity of paleoshore lines (Ece and Çoban, 1994; Yeniyol, 1992; Gençoğlu and İrkeç, 1994). Ece and Çoban (1994) suggested that sepiolite nodules formed diagenetically from magnesite cobbles, while sepiolite beds were precipitated in the central part of the same paleolake, and Mg and Si were derived from the ultrabasic rocks under alkaline and saline conditions.

The HFSE reflect provenance composition because of their immobility (Taylor and McLennan, 1985). These elements have a similar average concentration in detrital silicate-rich rocks as in PAAS but are depleted in limestone, dolostone, and sepiolitic and Mg-rich smectitic claystones, indicating immobility and dilution of the element in the lake (Figure 8b). The diluted lake water caused strong impoverishment of the elements during precipitation of the neoformed minerals. The average Zr content of detrital silicate-rich rocks (184 ppm) was similar to PAAS (210 ppm) and is generally 15 times greater than the other sample groups. The Zr/Hf ratio of detrital silicate-rich rocks (33) was similar to PAAS, NASC, and UC (42, 32, and 33, respectively), while the ratio was smaller in limestone (13), dolostone (14), and sepiolitic (22) and Mg-rich smectitic claystones (30). In addition, Zr had a positive correlation with HFSE in detrital silicate-rich rocks and limestones ($r^2 = 0.69$) and dolostone ($r^2 = 0.77$) whereas it was strongly negatively correlated with Mg-rich smectitic claystones ($r^2 = -0.96$). The mean Nb and Y contents of limestone (0.99, 1.36 ppm), dolostone (0.84, 1.16 ppm), and sepiolitic claystones (1.26, 1.62 ppm) were smaller than those of detrital silicate-rich rocks (16.37, 19.09 ppm) and PAAS (19, 27 ppm), respectively, showing that these elements were not concentrated in the neoformed minerals and were immobile. The HFSE contents and ratios indicated that neoformed minerals

https://doi.org/10.1346/CCMN.2011.0590306 Published online by Cambridge University Press

were formed under similar environmental conditions and may have been derived from a similar source.

Vanadium (V) concentrations were smaller than the levels in common shales and in the UCC. The V content of sepiolitic claystones ranged from 29 to 240 ppm, with an average of 79 ppm, similar to Mg-rich smectitic claystones; dolostone and limestone contained less but detrital silicate-rich rocks had more (average 104 ppm). Vanadium was enriched in organic-matter-rich shales deposited under reducing conditions. The V may also have been hosted by detrital silicate minerals (Stow and Atkin, 1987). The V/Cr ratio has been used as a paleo-oxygenation indicator in a number of studies. The average V/Cr values of some samples of limestone, dolostone, sepiolitic claystones, Mg-rich smectitic claystones, and detrital silicate-rich rocks were sometimes <2, which may indicate that the sediments were deposited under relatively oxidizing conditions, and sometimes >2, indicating that the sediments were precipitated under relatively anoxic conditions (Dill *et al*., 1988). Hence, these changes in the V/Cr ratio (from 0.11 to 6.28) may indicate that both types of conditions prevailed from time to time. Changing the depositional conditions also led to the Eu* and Ce* anomalies mentioned above. Organic matter-rich black sepiolitic claystones were formed under anoxic conditions while white sepiolite formed under oxic conditions. Precipitation of different colored sepiolite was related to water stratification and changing redox state in the deepest part of Miocene Sakarya basin. The black sepiolite beds contained nearly pure sepiolite and were overlain and sometimes underlain by brown sepiolite (Figure 3a). The two types of sepiolites were formed under dysaerobic conditions before and after the anoxia maximum. The anaerobic conditions were formed by large sulfate concentrations which originated from the ascending hydrothermal solutions rich in sulfate along the active fault system in the vicinity of the basin (Figures 1, 2), with water depth increasing progressively due to extension of the graben and basin subsidence (Ece and Çoban, 1994).

Helgeson *et al.* (1969) showed an equilibrium saturation diagram for the system CaO–MgO–CO_2–SiO_2–H_2O at 25ºC and 1 atm, with the field boundaries between sepiolite, dolomite, calcite, magnesite, and amorphous silica. The phase diagram showed the coexistence of sepiolite with calcite, dolomite, and amorphous silica (Figure 10). The chemical precipitation of Mg-rich smectite, then sepiolite, and later or contemporaneous precipitation of dolomite and sepiolite was consistent with the saturation diagram of Helgeson *et al*. (1969). The intimate mixture of dolomite and sepiolite suggests that the brine water might have had a composition close to the field boundary between dolomite and sepiolite, and continued concentration of dissolved brines by evaporation caused precipitation of dolomite and sepiolite. Mg may have been divided between dolomite and sepiolite. The partitioning of Mg in the lacustrine sediments, the tendency for Mg to form not only carbonate but also silicates, is unclear (Deocampo, 2010). He suggested that sulfate reduction and associated anaerobic oxidation of organic matter can contribute to dolomitization, largely through the rise in pH and alkalinity. The close relation of the organic-matter-rich sepiolitic claystones to dolostone supports this suggestion.

The absence of aragonite in the study area may be related to the low Mg/Ca ratio (<12) in the lake water (Jones and Deocampo, 2003), caused by the chemical precipitation of both sepiolite and dolomite. Mg-rich smectite was formed by chemical precipitation directly from alkaline lake water due to high pH (pH > 8.5) values and increased Mg and Si activity (Birsoy, 2002). High-silica solutions are most favored for the direct precipitation of sepiolite from solution.

The presence of a transformational relationship between sepiolite and trioctahedral smectite was also observed by Galán and Castillo (1984). The silica might be provided by volcanic ash or from the breakdown of the Mg-rich smectites or detrital silicate-rich rocks. Parry and Reeves (1968) believed that montmorillonite may have been the main source of silica for the neoformation of sepiolite in Texas, USA, as the lakes became more alkaline. The occurrence of an authigenic silicate mineral in the central part of the basin was interpreted to be a result of chemical interaction with saline, alkaline brine that changed with lake level. McLean *et al*. (1972) concluded that Pleistocene volcanic ash provided the main source of silica for the deposit. The increased Mg and Si contents were produced by dissolution of Lower to Middle Miocene pyroclastics in a lacustrine environment. The Mg may have been supplied by waters which percolated through the fractures of metadolomitic limestones (Figure 1).

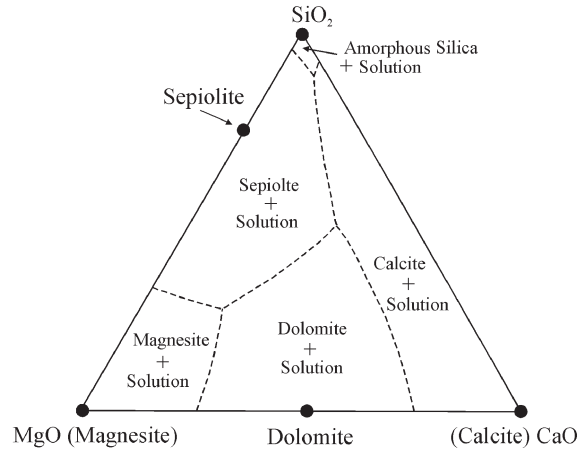

Figure 10. Phase diagram for the system CaO–MgO–CO_2–SiO_2–H_2O at 25ºC and 1 atm. (Helgeson *et al*., 1969).

https://doi.org/10.1346/CCMN.2011.0590306 Published online by Cambridge University Press

The sepiolite and Mg-rich smectite were the only magnesian-silica-rich argillaceous minerals present in the area, confirming the lack of detrital input among the sepiolite layers, the water supply of the lake, the SiO_2(aq), and Mg^{2+} cations leached from the Mg-rich smectite. A gradual increase in the Mg and silica content by evaporation of the lake water was caused by precipitation of Mg-rich smectite and then sepiolite; then sepiolite began to be deposited along with the dolomite. The silica activity alone was insufficient for dolomite precipitation. With the pH of the environment slightly acidic, sepiolite was not precipitated, and breakdown of silica increased under saturation with respect to amorphous silica (opal, opal-CT).

In SEM observations, silica (opal-A, opal-CT) cavities were surrounded by sepiolite (Figure 7g–i, Table 3), transitions from rims of silica compounds to sepiolite or *vice versa* were interpreted as representing a transformation reaction. Thin, long sepiolite fibers graded to thick, short sepiolite and then to more diffuse fibers near the edges of silica. Finally, the thick sepiolite fibers became more disordered. The Mg deficiency of the thick fibers (in contrast to the thin fibers) was determined by EDS analysis. This relation of silica minerals (*e.g.* opal-CT, moganite, quartz) with sepiolite may represent the gradual collapse of sepiolite structures, which mobilized Si while Mg precipitated as dolomite. The presence of calcite and the decrease in amount of dolomite in the upper level might have been due to an influx of fresher water or the development of an outlet from the lake, either of which would have caused a decrease in salinity of the Polatlı basin. The coexistence of calcite and sepiolite and filling of partially dissolved calcite crystals by sepiolite fibers may have been related to the equilibrium of Helgeson *et al*. (1969). If so, the calcite-sepiolite minerals were formed when fluid compositions were near the field boundaries between sepiolite and calcite. In the carbonate-containing sediments, dissolution of $CaCO_3$ led to pH values of ~8.0 (Weaver, 1989). Sepiolite may have formed contemporaneously with or just after dissolution of calcite.

An increase in silica precipitation, occurring as irregular and discontinuous layers, has been observed generally in the upper section and intervals of the sepiolite-rich layers. Some occurrences of Si compounds contained moganite. Bustillo (2002) stated that moganite occurs as a metastable phase that transforms to quartz (opal→ opal CT → quartz), if given sufficient time or changes in ambient conditions. Bustillo (2002) also claimed that moganite is abundant in arid, alkaline environments. The precipitation of chert layers containing moganite and quartz suggests that siliceous gel precipitated from solution during carbonate precipitation and/or after sepiolite precipitation from arid, alkaline environments under evaporitic regimes. The authigenic silicate mineral may have formed as a result of chemical interaction with a saline, alkaline brine that changed with lake levels and water stratification. The results suggest that distributions of authigenic silicate minerals in saline, alkaline lake deposits are related in a complex way to depositional and hydrologic processes and may be of limited utility in resolving lake-level changes in ancient lacustrine systems (Larsen, 2008).

Moganite-to-quartz transformation and opal-A/opal-CT transformation to Mg-poor to Mg-rich material (sepiolite) were observed in SEM and EDS analyses (Figure 7, Table 3). The Mg content of the thick, short-fiber sepiolite was smaller than longer sepiolite fibers near the Si compounds and sepiolite border. Esteban-Cubillo *et al*. (2008) found that, although sepiolite particles maintained their fibrous aspect, the crystalline framework of sepiolite collapsed when the fraction of leached Mg^{2+} was greater than or equal to 0.33, forming amorphous silica. Mineralogical studies (XRD, SEM-EDS) of the relation between Si compounds and sepiolite revealed different stages of organization, from opal-CT to microcrystalline quartz. Kent and Kastner (1985) proposed that the Mg^{2+} can be removed from suspensions containing amorphous silica at low temperatures by adsorption and precipitation of a Mg-hydrosilicate resembling sepiolite. The rate of sepiolite formation increases with increasing Mg^{2+} concentration, dissolved silica concentration, pH near 8, and temperature >10ºC (Kent and Kastner, 1985; Weaver, 1989).

CONCLUSIONS

Two types of mineral groups were determined in the Polatlı basin, based on mineralogical and chemical properties. The first group of minerals, consisting of neoformed minerals – calcite, dolomite, sepiolite, Mg-rich smectite, and silica compounds (opal-A, opal-CT, moganite, and quartz) – precipitated directly from lake water. Minerals in the second group, consisting of detrital silicate minerals, were derived from the catchment areas.

Neoformed silica compounds, filling cavities, formed from dissolution of sepiolite under weakly acidic conditions. Amorphous Si compounds were transformed to opal-CT → moganite → quartz. Although sepiolite habits maintained their fibrous aspect, transformation of sepiolite to silica caused collapse of long, thin sepiolite fibers to short, thick Mg-poor sepiolite.

Dissolution of calcite and/or dolomite and precipitation of sepiolite occurred contemporaneously. Some sepiolite developed as coatings on or around dolomite rhombs, indicating that they formed after precipitation of dolomite.

Trace element contents, some element ratios, and PAAS-normalized *REE* patterns of the neoformed minerals suggested a felsic source rock. The *REE*, TRE, LILE, and HFSE contents of neoformed minerals are lower overall than those of the detrital silicate minerals.

https://doi.org/10.1346/CCMN.2011.0590306 Published online by Cambridge University Press

The sepiolite deposits of a fluvio-lacustrine origin were formed in a closed, alkaline, shallow-lake environment. The Mg may have originated from Mg-rich smectites and metadolomitic rocks. The depositional environment was affected by varying oxic/anoxic conditions.

The MgO, Ba, Sr, V, and TRE contents are much smaller than those of the Eskişehir sepiolitic claystones, suggesting that the Eskişehir sepiolites may have been derived from a different source. The very large V content of the Eskişehir sepiolites points to a more anoxic environment than in the Polatlı basin.

ACKNOWLEDGMENTS

The present investigation was made possible through partial financial support by Selçuk University Scientific Research projects support program (054101007). The authors are indebted to two anonymous reviewers for their comments and to the editors for their careful and constructive suggestions which improved the quality of the manuscript.

REFERENCES

Anadón, P., Ghetti, P., and Gliozzi, E. (2002) Sr/Ca, Mg/Ca ratios and Sr and stable isotopes of biogenic carbonates from the Late Miocene Velona Basin (central Apennines, Italy) provide evidence of unusual non-marine Messinian conditions. *Chemical Geology*, **187**, 213–230.

Asutay, H.J., Küçükyaman, A., and Gözler, M.Z. (1989) Dağküplü (Eskişehir kuzeyi) ofiyolit karmaşığının stratigrafisi, yapısal konumu ve kümülatların petrografisi. *MTA Dergisi* **109**, 1–8.

Aubert, D., Stille, P., and Probst, A. (2001) REE fractionation during granite weathering and removal by waters and suspended loads: Sr and Nd isotopic evidence. *Geochimica et Cosmochimica Acta*, **64**, 1827–1841.

Bailey, S.W. (1980) Structures of layer silicates: Pp. 1–123 in: *Crystal Structures of Clay Minerals and Their X-ray Identification* (G.W. Brindley and G. Brown, editors), Monograph **5**, Mineralogical Society, London.

Bellanca, A., Karakaş, Z., Neri, R., and Varol, B. (1993) Sedimentology and isotope geochemistry of lacustrine dolomite-evaporite deposits and associated clays (Neocene, Turkey): environmental implication: *Mineralogica Petrographica Acta*, **XXXVI**, 245–264.

Birsoy, R. (2002) Formation of sepiolite-palygorskite and related minerals from solution. *Clays and Clay Minerals*, **50**, 736–745.

Blatt, H., Middleton, G., and Murray, R. (1972) *Origin of Sedimentary Rocks*. Prentice-Hall, New Jersey, USA, 634 pp.

Bonnot-Courtois, C. (1981) Géochimie des Teres Rares dans les principaus milieux de formation et de sédimentation des argiles. PhD thesis, Université Paris-Sud, Centre d'Orsay, Orsay, France, 277 pp.

Braun, J.-J., Pagel, M., Muller, J.-P., Bilong, P., Michard, A., and Guillet, B. (1990) Cerium anomalies in lateritic profiles. *Geochimica et Cosmochimica Acta*, **54**, 781–795.

Bustillo, M.A. (2002) Occurrence and significance of the moganite in silica rocks: A review. *Journal of Iberian Geology*, **28**, 157–166.

Class, C. and la Roex, A.P. (2008) Ce anomalies in Gough Island lavas – trace element characteristics of a recycled sediment component. *Earth and Planetary Science Letters*, **265**, 475–486.

Çoban, F. (2001) Ahiler (Sivrihisar-Eşkişehir) sepiyolitinin jeokimyasal özellikleri. *Yerbilimleri* **39**, 13–30.

Cox, R., Lowe, D.R., and Cullers, R.L. (1995) The influence of sediment recycling and basement composition on evolution of mudrock chemistry in the South-western United States. *Geochimica et Cosmochimica Acta*, **59**, 2919–2940.

Cullers, R.L. (1994) The controls on the major- and trace-element evolution on shales, siltstones and sandstone of Pennsylvanian-Permian age from uplifted continental blocks in Colorado to platform sediments in Kansas, USA. *Geochimica et Cosmochimica Acta*, **58**, 4955–4972.

Cullers, R.L. (1995) The controls on the major and trace-element evolution on shales, siltstones and sandstone of Ordovician to Tertiary age in wet mountains region, Colorado, USA. *Chemical Geology*, **123**, 107–131.

Cullers, R.L., Chaudhuri, S., Arnold, B., Lee, M., and Wolf, C.W. (1975) Rare earth distributions in clay minerals and in the clay-sized fractions of the Lower Permian Havensville and Eskridge shales of Kansas and Oklahoma. *Geochimica et Cosmochimica Acta*, **39**, 1691–1703.

Cullers, R.L., Basu, A., and Suttner, L.J. (1988) Geochemical signature of provenance in sand-mixed material in soils and stream sediments near the Tobacco Root batholiths, Montana, U.S.A. *Chemical Geology*, **70**, 335–348.

De Deckker, P., Chivas, A.R., and Shelley, J.M.G. (1988) Paleoenvironment of the Messinian Mediterranean ''Lago-Mare'' from Strontium and Magnesium in Ostracode shells. *Palaios*, **3**, 352– 358.

Deocampo, D.M. (2010) The geochemistry of continental carbonates. Pp. 1–59 in: *Carbonates in Continental Settings, Geochemistry, Diagenesis, and Applications* (A.M. Alonso-Zarza and L.H. Tanner, editors). Developments in Sedimentology, **62**, Elsevier, Amsterdam.

de Villiers, S. (1999) Seawater strontium and Sr/Ca variability in the Atlantic and Pacific oceans. *Earth and Planetary Science Letters*, **171**, 623–634.

Dill, H., Teschner, M., and Wehner, H. (1988) Petrography, inorganic, and organic geochemistry of Lower Permian carbonaceous fan sequences (''Brandschiefer Series'') – Federal Republic of Germany: constraints to their paleogeography and assessment of their source rock potential. *Chemical Geology*, **67**, 307–325.

Ece, Ö.İ. and Çoban, M. (1994) Geology, occurrence and genesis of Eskişehir sepiolites, Turkey. *Clays and Clay Minerals*, **42**, 81–92.

Ece, Ö.I., Suner, F., and Çoban, F. (2003) An approach to the origin of gypsum series in Upper Miocene succession, Eskişehir-Sivrihisar Lacustrine Basin, Turkey. *Neues Jahrbuch für Mineralogie – Monatshefte*, **11**, 481–502.

Esteban-Cubillo, A., Pina-Zapardiel R.J., Moya, S., Barba, M.F., and Pecharromán, C. (2008) The role of magnesium on the stability of crystalline sepiolite structure. *Journal of the European Ceramic Society*, **28**, 1763–1768.

Fleet, A.J. (1984) Aqueous and sedimentary geochemistry of the rare earth elements. Pp. 343–373 in: *Rare Earth Element Geochemistry* (P. Henderson, editor). Developments in Geochemistry, **2**. Elsevier, Amsterdam.

Florke, O.W., Martin, G.B., Bochum, R., and Wirth, R. (1991) Nomenclature of micro- and non-crystalline silica minerals, based on structure and microstructure. *Neues Jahrbuch fur Mineralogie – Abhandlungen*, **163**, 19–42.

Galán, E. and Castillo, A. (1984) Sepiolite-palygorskite in Spanish Tertiary basins: genetic patterns in continental environments. Pp. 87–124 in: *Palygorskite-sepiolite, Occurrences, Genesis and Uses* (A. Singer and E. Galán, editors). Developments in Sedimentology, **37**, Elsevier, Amsterdam.

Galán, E. and Ferrero, A. (1982) Palygorskite-sepiolite clays of

https://doi.org/10.1346/CCMN.2011.0590306 Published online by Cambridge University Press

Lebrija, southern Spain. *Clays and Clay Minerals*, **30**, 191–199.

Gençoğlu, H. and İrkeç, T. (1994) Eskişehir-Sivrihisar civarındaki sedimanter sepiyolit oluşumlarının ortamsal yorumu. *Türkiye Jeoloji Kurultay Bülteni*, **9**, 281–296.

Gromet, L.P., Dymek, R.F. Haksin, L.A., and Korotev, R.L. (1984) The "North American shale composite": its compilation, major and trace element characteristics. *Geochimica et Cosmochimica Acta*, **48**, 2469–3482.

Helgeson, H.C., Harold, C. Garrels, R.M., Robert, M., and Mackenzie, F.T. (1969) Evaluation of irreversible reactions in geochemical processes involving minerals and aqueous solutions – II. Applications: *Geochimica et Cosmochimica Acta*, **33**, 455–481.

Jackson, M.L. (1975) *Soil Chemical Analysis – Advanced Course*: 2nd ed., published by the author, Madison, Wisconsin, USA, 895 pp.

Jagoutz, E., Palme, H., Baddenhausen, H., Blum, K., Cendales, M., Dreibus, G., Spottel, B., Lorenz, V., and Wanke, H. (1979) The abundances of major, minor and trace elements in the earth's mantle as derived from primitive ultramafic nodules. Proceedings of the Lunar and Planetary Science Conferece No 10. *Geochimica et Cosmochimica Acta, Supplement* **11**, 2031–2050.

Jenner, G.A. (1996) Trace element geochemistry of igneous rocks: geochemical nomenclature and analytical geochemistry. Pp. 51–77 in: *Trace Element Geochemistry of Volcanic Rocks: Applications for Massive Sulfide Exploration* (D.A. Wyman, editor). *Geological Association of Canada Short Course Notes*, **12**.

Jones, B.F. and Deocampo, D.M. (2003) Saline lakes. In: *Surface and Ground Water, Weathering, Erosion and Soils* (J.I. Drever, editor). Treatise on Geochemistry, **5**, pp. 393–424.

Kabata-Pendias, A. and Mukherjee, A. (2007) *Trace Elements from Soil to Human*. Springer, Science Publishing, Amsterdam, 550 pp.

Kabata-Pendias, A. and Pendias, H. (2001) *Trace Elements in Soils and Plants*, 3rd edition. CRC Press, Boca Raton, Florida, USA, 413 pp.

Kadir, S., Baş, H., and Karakaş , Z. (2002) Origin of sepiolite and loughlinite in a Neocene volcano-sedimentary lacustrine environment, Mihalıçık-Eskişehir, Turkey. *The Canadian Mineralogist*, **40**, 1091–1102.

Karakaya, N., Karakaya, M.Ç., Temel, A., Küpeli, Ş., and Tunoğlu, C. (2004) Mineralogical and chemical characterization of the sepiolite occurrences at Karapınar (Konya Basin, Turkey). *Clays and Clay Minerals*, **52**, 495–510.

Kent, D.B. and Kastner, M. (1985) Mg^{2+} removal in the system Mg^{2+}-amorphous SiO_2-H_2O by adsorption and Mg-hydroxysilicate precipitation. *Geochimica et Cosmochimica Acta*, **49**, 1123–1136.

Larsen, D. (2008) Revisiting silicate authigenesis in the Pliocene–Pleistocene Lake Tecopa beds, southeastern California: depositional and hydrological controls. *Geosphere*, **4**, 612–639.

Mayayo, M.J., Bauluz, B., López-Galindo, A., and González-López, J.M. (1996) Mineralogy and geochemistry of the carbonates in the Calatayud basin (Zaragoza, Spain). *Chemical Geology*, **130**, 123–136.

Mayayo, M.J., Torres-Ruíz, J., González-López, J.M., López-Galindo, A., and Bauluz, B. (1998) Mineralogic and geochemical characterization of the sepiolite/Mg-rich smectite deposits at Mara (Calatayud basin, Spain). *European Journal of Mineralogy*, **10**, 367–383.

McLean, S., Allen, B., and Craig, J. (1972) The occurrence of sepiolite and attapulgite on the Southern High Plains. *Clays and Clay Minerals*, **20**, 143–149.

McLennan, S.M. (1989) Rare earth elements in sedimentary rocks: influence of provenance and sedimentary processes. Pp. 169–190 in: *Geochemistry and Mineralogy of Rare Earth Elements* (B.R. Lipin and G.A. McKay, editors). Reviews in Mineralogy, **21**, Mineralogical Society of America, Washington, D.C.

McLennan, S.M. and Taylor, S.R. (1991) Sedimentary rocks and crustal evolution: tectonic setting and secular trends. *Journal of Geology*, **99**, 1–21.

McLennan, S.M., Nance, W.B., and Taylor, S.R. (1980) Rare earth element-thorium correlation in sedimentary rocks, and the composition of the continental crust. *Geochimica et Cosmochimica Acta*, **44**, 1833–1839.

Moore, C.L. (1998) Evolution of regolith development and element mobility during weathering using isocon technique. *Geological Society of Australia, Special Publication*, **20**, 141–147.

MTA (2001) 1:500.000 scale map. Prepared by Geological research Department of the General Directorate of Mineral Research and Exploration.

Nemecz, E. (1981) *Clay Minerals*. Akademia Kiado, Budapest, 547 pp.

Parry, W. and Reeves, C. (1968) Sepiolite from pluvial Mound Lake, Lynn and Terry Counties, Texas. *American Mineralogist*, **53**, 884–993.

Post, J.L. (1978) Sepiolite Deposits of the Las Vegas, Nevada Area. *Clays and Clay Minerals*, **26**, 58–64.

Santiago Buey, C., Suárez Barrios, M., García-Romero, E., and Doval Montoya, M. (2000) Mg-rich smectite Precursor phase in the Tagus Basin, Spain. *Clays and Clay Minerals* **48**, 366–373.

Saunders, A.D., Tarney, J., Marsh, N.G., and Wood, D.A. (1980) Ophiolites as ocean crust: a geochemical approach. Pp. 193–204 in: *Ophiolites: Proceedings of the International Ophiolite Symposium* (A. Panayiotou, editor). Ministry of Agriculture and Natural Resources. Geological Survey Department, Cyprus.

Schilling, J.G. (1973) Iceland Mantle Plume: geochemical study of Reykjanes ridge. *Nature* **242**, 565–571.

Stow, D.A.V. and Atkin, B.P. (1987) Sediment facies and geochemistry of Upper Jurassic mudrocks in the central North Sea area. Pp. 797–808 in: *Petroleum Geology of North West Europe* (J. Brooks and K. Glennie, editors). Graham and Trotman, London.

Taylor, S.R. and McLennan, S.M. (1985) *The Continental Crust: its Composition and Evolution*. Blackwell, Oxford, UK, 312 pp.

Temel, A. and Gündoğdu, M.N. (1996) Zeolite occurrences and erionite-mesothelioma relationship in Cappadocia region, Central Anatolia, Turkey. *Mineralium Deposita*, **31**, 539–547.

Temel, A., Yürür, T., Alıcı, P., Varol, E., Gourgaud, A., Bellon, H., and Demirbağ, H. (2010) Alkaline series related to Early-Middle Miocene intra-continental rifting in a collision zone: an example from Polatlı, Central Anatolia, Turkey. *Journal of Asian Earth Sciences*, **38/6**, 289–306.

Terkado, Y. and Fujitani, T. (1998) Behavior of rare earth elements and other trace elements during interactions between acidic hydrothermal solutions and silicic volcanic rocks, southwestern Japan. *Geochimica et Cosmochimica Acta*, **62/11**, 1903–1917.

Torres-Ruíz, J., Lopez-Galindo, A., González-Lopez, J.M., and Delgado, A. (1994) Geochemistry of Spanish sepiolite-palygorskite deposits: Genetic considerations based on trace elements and isotopes. *Chemical Geology*, **112**, 221–245.

Varol, E., Temel, A, Gourgaud A., and Bellon, H. (2007) Early Miocene adakite-like volcanism in the Balkuyumcu region, central Anatolia, Turkey. *Petrology and Geochemistry Journal of Asian Earth Sciences* **30**, 613–628.

Weaver, C.E. (1989) *Clays, Muds and Shales*. Developments in

https://doi.org/10.1346/CCMN.2011.0590306 Published online by Cambridge University Press

Sedimentology, **44**, Elsevier, Amsterdam, 819 pp.
Weaver, C.E. and Pollard L.D. (1973) *The Chemistry of Clay Minerals*. Developments in Sedimentology, **XX**, Elsevier Science Publishing, Amsterdam, 213 pp.
Whitney, D.L. and Evans, B.W. (2010) Abbreviations for names of rock-forming minerals. *American Mineralogist*, **95**, 185–187.
Wise, S.W. and Kelts, K.R. (1972) Inferred diagenetic history of a weakly silicified Deep Sea Chalk Trans Gulf Coast. *Association of Geological Societies*, **22**, 177–203.
Wronkiewicz, D.J. and Condie, K.C. (1987) Geochemistry of Archean greywackes from Wyoming Supergroup, South Africa: source-area weathering and provenance. *Geochimica et Cosmochimica Acta*, **51**, 2401–2416.
Wronkiewicz, D.J. and Condie, K.C. (1989) Geochemistry and provenance of sediments from the Pongola Supergroup, South Africa: evidence for a 3.0 Ga old continental craton. *Geochimica et Cosmochimica Acta*, **53** 1537–1549.
Wronkiewicz, D.J. and Condie, K.C. (1990) Geochemistry and mineralogy of sediments from the Ventersdrop and Transvaal Supergroups, South Africa: cratonic evolution during the early Paleozoic. *Geochimica et Cosmochimica Acta*, **54**, 343–354.
Yalçın, H. and Bozkaya, Ö. (1995) Sepiolite-palygorskite from the Hekimhan Region (Turkey). *Clays and Clay Minerals*, **43**, 705–717.
Yalçın, H. and Bozkaya, Ö. (2004) Ultramafic-rock-hosted vein sepiolite occurrences in the Ankara Ophiolitic Mélange, central Anatolia, Turkey. *Clays and Clay Minerals*, **52**, 227–239.
Yeniyol, M. (1986) Vein-like sepiolite occurrence as a replacement of magnesite in Konya, Turkey. *Clays and Clay Minerals*, **34**, 353–356.
Yeniyol, M. (1992) Geology, mineralogy and genesis of Yenidoğan (Sivrihisar) sepiolite deposit. *Mineral Research and Exploration Bulletin of Turkey*, **114**, 71–84.

(*Received 27 February 2010; revised 5 September 2011; Ms. 410; A.E. R.J. Pruett*)

https://doi.org/10.1346/CCMN.2011.0590306 Published online by Cambridge University Press